Functional Analysis of Spinal Commissural Neurons in Zebrafish

Chie Satou

DOCTOR OF PHILOSOPHY

Department of Physiological Science, School of Life Science,

The Graduate University for Advanced Studies

2009

CONTENTS

GENERAL INTRODUCTION

Movements are essential for life in virtually all animals. To move properly, the nervous system needs to produce appropriate patterns of motoneuron activation, and in vertebrates, neuronal circuits within the spinal cord play a pivotal role in this task. In this sense, spinal neuronal circuits have been the subject of intense investigation (Kiehn, 2006; Goulding, 2009). While much progress has been made, the relative complexity of mammalian spinal circuits has made studies of how spinal locomotor circuits generate appropriate motor outputs, such as walking or running, more difficult.

One way to make questions more tractable is to use animals in which the spinal locomotor circuitry is simpler. In this study, I use the larval zebrafish model system to study spinal locomotor circuits. The zebrafish is best known as a model organism for studies of development, but recently it has become an important model for studies of neuronal function (Fetcho, 2007; Fetcho et al., 2008). In addition to their relatively simple nervous system, the zebrafish has additional advantages: namely, transparency of the body and amenability to genetics. These two features make it possible to generate fish in which subclasses of neurons are labeled by fluorescent protein such as GFP (green fluorescent protein) (Higashijima, 2008). Though relatively simple, the zebrafish spinal cord contains many cell types (Hale et al., 2001; Higashijima et al., 2004a; Higashijima et al., 2004b). Visualization of particular classes of neurons by GFP has proven a very powerful approach for studying classes of neurons morphologically and physiologically in detail (Higashijima et al., 2004c; Kimura et al., 2006).

In any vertebrate, coordinated movements of the left and right sides of the body are very important in any movement. Commissural neurons are those that project to the opposite side of the spinal cord. Firing of commissural neurons impacts the activity of

their post-synaptic targets located on the opposite side, and thus, commissural neurons must play a critical role in coordinating movements of the body (Roberts, 2000; Kiehn and Butt, 2003). However, we have little knowledge of how many types of commissural neurons are involved in the coordination of movements and how these different types of commissural neurons can generate proper movements.

Here, I employed the GFP-labeling technique, and studied several classes of commissural neurons in larval zebrafish. In the study that is described in Chapter 1, I examined commissural neurons that derive from a region of spinal cord expressing the *dbx1* gene. Neurons derived from *dbx1*-expressing cells turned out to be heterogeneous. I will present my morphological analysis of these neurons and my physiological analysis of one class of inhibitory neuron within the *dbx1*-labeled population.

I also looked for transgenic fish in which only one class of neuron is unambiguously labeled by GFP. By screening enhancer-trap lines, I found one such transgenic fish. In Chapter 2, I will present my detailed morphological, physiological, and functional analysis of the GFP-labeled neurons in the enhancer-trap line.

CHAPTER I :

Morphological and Electrophysiological Analysis of Spinal V0 Neurons

SUMMARY

dbx1 is a homeobox gene that is expressed in neuronal progenitors located in the intermediate region of the developing spinal cord. Neurons that derive from dbx1-expressing progenitors (V0 neurons) are predominantly commissural in amniotes, but their fine morphological and physiological properties are still largely unknown. Thus, I am attacking this issue using the zebrafish model system. Using transgenic zebrafish lines that express fluorescent proteins in *dbx1*-expressing cells and/or their progeny, I show that zebrafish V0 neurons are all commissural, consisting of both excitatory and inhibitory neurons. Morphologically, excitatory neurons are heterogeneous. Based on the trajectories of axons on the contralateral side of the body, V0 excitatory neurons can be subdivided into three groups: ascending, bifurcating and descending neurons. According to their dendritic morphologies, ascending and descending neurons can be further subdivided into two groups: multipolar and unipolar. By contrast, V0 inhibitory neurons are relatively homogeneous in morphology. Morphological features of V0 inhibitory neurons include: unipolar somata with dendrites coming off from the primary process, and bifurcating axons on the contralateral side of the body. The axonal length of V0 inhibitory neurons, on average, is shorter than that of V0 excitatory neurons. I also examined the firing patterns of V0 inhibitory neurons during fictive swimming. They tend to fire in phase with ventral root activity, suggesting that they are involved in reciprocal inhibition of body movements during swimming. The results of the present study will provide useful information for comparative studies of spinal neuronal circuits in other vertebrate species, including amniotes.

INTRODUCTION

In vertebrates, neuronal circuits located within the spinal cord are responsible for generating elemental patterns of motor activity, such as walking and swimming (Brown, 1914; Grillner and Zangger, 1979; Kjaerulff and Kiehn, 1996). Given this fact, it is clearly important to understand how spinal neuronal circuits are organized and function. To help studies of spinal circuitry, it is crucial to be able to identify cell types and to investigate the physiological roles of the neurons. However, because there are many types of neurons, very often intermingled within the spinal cord, it has been difficult to reproducibly identify cell types using just electrophysiological and anatomical approaches alone.

Recent molecular genetic studies directed toward understanding the development of spinal neuronal circuits have provided a new way to identify cell types. The studies have revealed that transcription factors are expressed in a subset of neuronal progenitors or postmitotic neurons in the developing spinal cord (Briscoe et al., 2000). These transcription factors are presumed to play important roles in establishing various neuronal types. Thus, it is possible to utilize the expression of these transcription factors to identify and record from different cell types in the spinal cord.

In the developing spinal cord, the ventral half is important for producing locomotion (Kjaerulff and Kiehn, 1996; Cina and Hochman, 2000; Dai et al., 2005) and it can be divided into five distinct domains based on the expression patterns of several transcription factors (Jessell, 2000; Shirasaki and Pfaff, 2002). These five domains are

called p3, pMN, p2, p1, and p0 from ventral to dorsal, as shown in Figure 1. Neurons

that derive from these progenitor domains express different sets of transcription factors,

and are called V3, motor (motoneurons derive from pMN domain), V2, V1, and V0

neurons, respectively (Moran-Rivard et al., 2001; Al-Mosawie et al., 2007; Peng et al.,

2007). Differential expression of transcription factors in progenitor cells or postmitotic

neurons has proven useful for the identification of cell types (Saueressig et al., 1999;

Seo et al., 1999; Goulding and Lamar, 2000; Goulding, 2009). In particular, the usage

of transgenic animals expressing fluorescent proteins has enabled live visualization of

the cells during experiments (Higashijima et al., 2004c; Kimura et al., 2006; Kwan et al.,

2009).

Dbx1 is a homeobox gene that is exclusively expressed in p0 progenitors

(Pierani et al., 2001; Gribble et al., 2007). In this study, I investigated neurons that

derive from *dbx1*-expressing progenitors (V0 neurons). There are two aims in the

present study. The first aim is to investigate the organization of zebrafish locomotor

circuits. There is a long history of investigation into the spinal locomotor circuits of

aquatic vertebrates, mainly in frog tadpoles and adult lamprey. These classic studies

have provided valuable information about the basic patterns of neuronal organization

that generate swimming (Grillner et al., 1998; Roberts, 2000). Spinal locomotor circuits

in zebrafish are currently less well understood, but I expected that studying them with

modern methodology, such as genetic labeling of neurons, would enable researchers to

perform morphological and physiological analyses in finer resolution, and thus would

not just repeat tadpole/lamprey studies but uncover new findings. Indeed, aided by the

genetic labeling of neurons, McLean et al. recently revealed new information regarding

how spinal locomotor circuits are organized (McLean et al., 2007; McLean et al., 2008).

The second aim is to provide an insight into general feature of the vertebrate spinal cord from the study of zebrafish spinal neuronal circuitry. The expression patterns of transcription factors in the developing spinal cord are highly conserved across vertebrate species. This has allowed us to perform a cross-species comparison of neuronal types based on the expression of transcription factors. Previous studies in V1 neurons and V2a neurons (an excitatory subset of V2 neurons) in zebrafish and mice have revealed marked similarity in the features of these neurons between the two species (Saueressig et al., 1999; Higashijima et al., 2004c; Sapir et al., 2004; Kimura et al., 2006; Crone et al., 2008; Crone et al., 2009). These studies point to the usefulness of zebrafish for comparative studies of cell types in the spinal cord. Furthermore, zebrafish can be important for considering functional organization of spinal locomotor circuits in vertebrates. It is assumed that limb-based locomotor circuits have been built up upon swimming-based locomotor circuits with many modifications during evolution (Goulding, 2009). In this sense, swimming-based locomotor circuits and limb-based locomotor circuits may share some basic components. Thus, elucidating zebrafish neuronal circuits labeled by specific transcription factors could provide insights into the general organization of locomotor circuits in vertebrates.

Here, I show that zebrafish V0 neurons are commissural and are comprised of both excitatory and inhibitory neurons. Morphologically, V0 excitatory neurons are heterogeneous, while V0 inhibitory neurons are relatively homogeneous. My physiological analysis strongly suggests that V0 inhibitory neurons are involved in the reciprocal inhibition of body movements during swimming. In mice, V0 neurons are composed of excitatory and inhibitory commissural neurons, with inhibitory ones implicated in the left-right alteration of limb movements (Lanuza et al., 2004). Thus, V0

inhibitory neurons in zebrafish and mice are remarkable similar in function. Further

examination of zebrafish V0 neurons in the future will reveal a more complete picture

of V0 neurons in this species, and will provide a solid platform for phylogenetic studies.

MATERIALS and METHODS

Animals

Zebrafish adults, embryos and larvae were maintained at 28.5°C. Experiments were performed at room temperature (22-28°C). All procedures were performed in compliance with the guidelines approved by the animal care and use committees of the National Institutes of Natural Sciences. Animals were staged according to hours post fertilization (hpf) or days post fertilization (dpf).

DNA construction and generation of transgenic fish

To manipulate BAC DNA, the BAC homologous recombination technique developed by the Copeland lab (Lee et al., 2001) was used. The template for introducing DNA consists of EGFP, a poly(A) signal from bovine growth hormone (BGH), and a Kanamycin resistant gene (Km^r) in this order (Kimura et al., 2006). For DsRed and Cre constructs, 0.6 kb of the zebrafish hsp70 promoter (Halloran et al., 2000) was inserted in front of DsRed (or Cre) to enhance the expression level of DsRed (or Cre) in transgenic fish. The template DNA for DsRed constructs consists of hsp, loxP, DsRed, loxP, BGH poly(A), Km^r, EGFP, and simian virus 40 (SV40) polyA in this order (Kimura et al., 2006). A fusion protein of Cre-mCherry-NLS (nuclear localization signal) was used as Cre recombinase. For this, Cre (a gift from Drs. T. Sato and H. Okamoto, RIKEN), mCherry (a gift from Dr. R. Tsien, UCSD), and NLS (synthesized DNA) were fused with their reading frame being in-frame. The purpose of adding

mCherry was to identify transgenic fish with the presence of mCherry fluorescence. NLS was added to facilitate nuclear transportation of the fusion protein. The template DNA for Cre constructs consists hsp, Cre-mCherry-NLS, BGH poly(A), and Km^r in this order. The BAC DNAs used in this study were the following; zK17G17 for *dbx1b,* zK76N24 for *glyt2* (*glycine transporter 2*) (McLean et al., 2007), and zK145P24 for *vglut2a* (*vesicular glutamate transporter 2a*). These BAC clones were obtained from RZPD (Berlin, Germany). BAC DNA constructs generated in this study were the following; *dbx1b*:GFP, *dbx1b*:loxP-DsRed-loxP-GFP, *glyt2*: loxP-DsRed-loxP-GFP, *vglut2a*: loxP-DsRed-loxP-GFP. All targeting DNA fragments for homologous recombination were prepared by PCR. Homology arm sequences (included in the primers) used for homologous recombination are listed in Table 1.

For the generation of the *gfap*:dTomato construct, approximately 7.3 kb of the 5′ upstream sequence of zebrafish *gfap*, that was shown to be capable of driving gene expression in astrocytes (Bernardos and Raymond, 2006) was PCR-amplified from a zebrafish BAC containing the *gfap* gene, zK15N1 (obtained from RZPD). The amplified gfap promoter, dTomato (a gift from Dr. R. Tsien), and BGH polyA were placed in this order in the pT2KXIGdin vector that has zebrafish Tol2 transposable elements (Kawakami, 2004; Urasaki et al., 2006).

Microinjection of BAC DNA for the generation of transgenic fish was performed as described previously (Kimura et al., 2006). Microinjection of Tol2-based plasmid DNA was performed as described previously (Urasaki et al., 2006). I established two transgenic lines for *dbx1b*:GFP, one for *dbx1b*:loxP-DsRed-loxP-GFP, two for *vglut2a*: loxP-DsRed-loxP-GFP, four for *dbx1b*:Cre, over twenty for

glyt2:loxP-DsRed-loxP-GFP and three for *gfap*:dTomato. For each construct, the line having the brightest fluorescence was used in this study. The transgenic fish generated in this study are represented in Figure 2.

Stochastic labeling of V0 neurons with GFP

For stochastic expression of GFP in V0 neurons, BAC DNA of *vglut2a*: loxP-DsRed-loxP-GFP (for glutamatergic neurons) or *glyt2*:loxP-DsRed-loxP-GFP (for glycinergic neurons) was injected into one-cell stage embryos of Tg[*dbx1b*:Cre] stable transgenic fish. Laval fish having GFP expression in a small number of neurons were selected using a fluorescent dissecting microscope. GFP-labeled neurons were imaged in the living fish by confocal microscopy at 5 dpf.

In situ hybridization and antibody staining

In situ hybridization was performed using a standard protocol. For double in situ hybridization, one probe was labeled with digoxigenin and detected by alkaline phosphatase-conjugated anti-digoxigenin antibody and an HNPP fluorescent detection set (all reagents were from Roche, Penzberg, Germany). The other probe was labeled with fluorescein (Roche) and detected by peroxidase-conjugated anti-fluorescein antibody (Roche) and a TSA kit with Alexa Fluor 647 (Invitrogen) according to the manufacturer's instructions. Antibody staining was performed as described previously (Higashijima et al., 2004b). The anti-GAD65/67 antibody (GC3108, Sigma) was used.

The secondary antibody used was Cy5-conjugated anti-mouse antibody (Jackson ImmunoResearch).

Sectioning

Samples were fixed in 4% paraformaldehyde, soaked in 30% sucrose, and mounted in Tissue-Tek O.C.T. compound (Sakura, Torrance, CA). Twenty-five-micron frozen sections were generated with a Leica E2800 cryostat.

Electrophysiology

Electrophysiological recordings from glycinergic V0 neurons were performed using dual transgenic fish for Tg[*dbx1b:*Cre] and Tg[*glyt2*:loxP-DsRed-loxP-GFP]. In early experiments, fish that had transient expression of GFP in V0 glycinergic neurons were also used. Such fish were obtained by injecting the *glyt2*:loxP-DsRed-loxP-GFP DNA construct into embryos of Tg[*dbx1b*:Cre] transgenic fish. Fish (3-4 dpf) were paralyzed by soaking them in 1 mg/ml of α-bungarotoxin (Sigma, St. Louis, MO) or d-tubocurarine (0.1 mg/ml in distilled water; Sigma) for 5-15 min. For animals that were immobilized with d-tubocurarine, the same reagent at a concentration of 0.01 mM was added to the recording solution throughout the experiments. Embryos were then pinned to a Sylgard-lined glass-bottomed Petri dish with short pieces of fine tungsten wire pushed through the notochord. Embryos were then covered with extracellular recording solution that contained (in mM): 134 NaCl, 2.9 KCl, 1.2 $MgCl_2$, 2.1 $CaCl_2$, 10 HEPES, and 10 glucose, adjusted to pH 7.8 with NaOH (Drapeau et al., 1999). The skin

in the middle region of the body was removed with a pair of forceps. Three to four

segments (between the 10th and 14th segments) of superficial muscle fibers that

covered the spinal cord were carefully removed manually with a fine tungsten wire. To

clear away deeper muscle fibers, I bathed the preparation in recording solution that

contained collagenase (0.03%; Sigma). After clearing away the remaining muscle fibers

from the spinal cord, I rinsed off the collagenase solution and then removed the rest of

the skin to facilitate ventral root (VR) recordings (see below). For all electrophysiology

experiments, the preparations were observed using a water immersion objective (40x;

numerical aperture, 0.80; Olympus, Tokyo, Japan) on an upright microscope (BX51WI;

Olympus) fitted with differential interference contrast optics.

Extracellular recording techniques were used to monitor the activity of

peripheral nerves (ventral root; VR) during fictive swimming. Recording sites were

typically two to six segments rostral from the patch-electrode recording site.

Extracellular suction electrodes were pulled on a Flaming-Brown micropipette puller

(P-97; Sutter Instruments, Novato, CA) from borosilicate glass (Model GC150F-7.5,

ID=0.86 mm, OD=1.5mm; Harvard Apparatus). These micropipettes were broken to

create tip diameters of about 20–50 mm and polished using a microforge (Model

MF-830, Narishige). These electrodes were filled with d-tubocurarine -free extracellular

recording solution. The tip of the suction electrode was positioned at the dorsoventral

midpoint of a myotomal cleft where the skin had been removed, and a light suction was

applied to ensure a tight seal with the underlying muscle tissue and peripheral nerves.

Patch electrodes were pulled 15-25 $M\Omega$ resistances from the same glass on the

same puller and filled with patch solution (in mM; 118.55 Kgluconate, 4.35 KCl,

2.36 $MgCl_2$, 10 HEPES, 10 EGTA, and 4 Na_2ATP, adjusted to pH 7.2 with KOH).

The calculated chloride reversal potential was -69 mV. The calculated liquid junction

potential I corrected for was 15.2 mV. Patch electrodes were advanced into the exposed

portion of the spinal cord using a motorized micromanipulator while maintaining

positive pressure (25–50 mm Hg) via a pneumatic transducer (Model DPM-1B, Bio-Tek

Instruments) to avoid tip clogging. When the tip of the micropipette was in close

proximity to the soma of the targeted cell, a $G\Omega$ seal was obtained by applying gentle

suction. A holding current of -60 mV was applied once the micropipette had become

cell attached. Whole-cell recordings were obtained by penetrating the membrane using

gentle suction pulses. Standard corrections for bridge balance and capacitance were then

applied.

Whole cell and peripheral nerve recordings were acquired using a Multi-Clamp

700B amplifier, a Digidata series1322A digitizer and pClamp 9 or 10 software (the

equipment and the software were from Molecular Devices). Electrical signals from

spinal cells were filtered at 10 kHz and digitized at 66.7 kHz with a gain of 10

(Feedback resistor, 500 $M\Omega$). The recordings were accepted for data analysis if the

resting membrane potential of GFP-positive neurons was more negative than -45

mV. Extracellular signals from peripheral nerves were recorded in current clamp mode

at a gain of 1,000, with the low and high frequency cutoff set at 100 and 4,000 Hz,

respectively.

Fluorescent dye (0.02% Alexa Fluor 594 hydrazide or 0.0025% Alexa Fluor

647 tris salt, Invitrogen) was included in the patch solution so that I could assess the

morphologies of the cells immediately after the recordings. Images were acquired with a

CCD camera (XC-ES51; Sony, Tokyo, Japan) and a frame grabber (LG3; Scion, Frederick, MD), or a FV300 confocal unit (Olympus).

Fictive swimming often occurred spontaneously, but could also be elicited by applying flashlight or a brief electrical stimulus (0.5-1 ms in duration at 1–10 V) delivered via a tungsten electrode placed near otolith.

Data analysis

All data were analyzed off-line using DataView (W. Heitler, University of St Andrews, St. Andrews, UK), Excel (Microsoft, Settle, WA) and Matlab (The MathWorks, Natick, MA). Ventral root cycles were full-wave-rectified and smoothed in DataView (half window 1 msec). The onset and offset of the burst event was determined when the rectified signal exceeded 1.5 times the average noise level between bursts. A cycle time (T) of motor nerve activity started at the mid time-point of the burst event and ended at the mid time-point of the next burst event. Spike timing in the recorded neurons was defined as the time point of the peak of each action potential. Because the recordings from the ventral roots (VR) and a neuron were in different body segment, the timing of the VR needed to be corrected for further analysis. To know the delay of the motor activity along the rostro-caudal axis during fictive swimming, I recorded fictive motor patterns from motor nerves at two different places. During typical fictive swimming (20-30 Hz of bending frequency), the calculated average rostro-caudal delay was 0.79 ms for a single body segment. Thus, this value was used for the correction. For example, when the recording site of VR was 5 segments rostral to the patch recording site, a 3.95 ms (0.79 ms times 5) timing shift was applied to the VR data.

Circular analysis was performed to examine the phasing of recorded neuron firing during fictive locomotion (Zar, 2009). Zero timing for each event was defined as the mid time-point of the event (Fig. 9E). The phase value (Φ) of each spike was calculated with regard to mid time-point of the burst event. The phase calculation was done as shown in Figure 9E by dividing the latency (L) between spikes and the starting point of the nearest cycle (mid time-point of the burst) by the cycle period (T). The mean phase, $\overline{\Phi}$ of the individual phases Φ, was calculated using the formula:

$$\tan\overline{\Phi} = \frac{Y}{X},$$ (1)

where

$$X = \frac{\sum_{i=1}^{n} \cos \Phi_i}{n}$$ (2)

and

$$Y = \frac{\sum_{i=1}^{n} \sin \Phi_i}{n}.$$ (3)

In Equations (2) and (3), n was the number of cycles in the sample.

In Figures 9F and G, the phase values of spikes have been plotted on a circle representing the interval of possible phases from 0 to 1. The phase values 0 and 1 are equivalent and reflect synchrony, whereas 0.5 is equivalent to alternation. The mean phase $\overline{\Phi}$ is indicated by the direction of the vector originating from the center of the circle (Figs. 9F-H). For each cell, more than 20 burst events in which the recorded

V0-iB fired were analyzed. Cells that did not fire during fictive swimming were not analyzed in this study.

RESULTS

Visualization of V0 neurons in live zebrafish

V0 neurons are those that derive from neuronal progenitors expressing the homeodomain protein Dbx1. My initial approach was to utilize the promoter/enhancer of *dbx1* to drive GFP expression in V0 neurons. Although Dbx1 is a gene that is predominantly expressed in progenitor cells (p0 progenitors), I expected that not only p0 progenitors but also postmitotic V0 neurons would be labeled by GFP because of the stability of GFP protein. In the zebrafish genome, two *dbx1* orthologs, dbx1a and dbx1b, are present (Gribble et al., 2007). This is presumably due to genome wide duplication in teleost lineages during evolution. Expression patterns of *db*x1a and *dbx1b* in the spinal cord appear virtually identical (Seo et al., 1999; Gribble et al., 2007). In this study, I chose to use *dbx1b*, as a suitable BAC clone (zK17G17; an ~212 kb insert, of which ~93 kb was upstream), was available for this gene. Using the BAC, I generated Tg[*dbx1b*:GFP] transgenic fish (Fig. 3A; 2.5 dpf). In addition to expression in the spinal cord, GFP expression was also observed in the brain, consistent with the known expression pattern of *dbx1b* (Seo et al., 1999). I first examined whether *dbx1b* expression was accurately recapitulated by *gfp* in the transgenic fish. For this purpose, dual in situ hybridization with *dbx1b* and *gfp* was performed. As shown in Figure 3B1-B3, mRNA expression of *gfp* and *dbx1b* overlapped, confirming that *dbx1b* expression was accurately recapitulated by *gfp* in the transgenic fish.

Weak GFP expression was first detected at 13 hpf in Tg[*dbx1b*:GFP] fish (data

not shown). Figure 3C shows confocal stacked image of the cross section at 36 hpf.

GFP expression was observed in a stripe-like pattern (Fig. 3C). Within this stripe

(p0/V0 domain), both *dbx1b*-expressing p0 progenitors and postmitotic neurons derived

from p0 progenitors (V0 neurons) were present, as ventrally-extending GFP positive

processes were already recognized at this stage (arrow in Fig. 3C). Postmitotic neurons

are located in the lateral region of the stripe at this stage. Figure 3D shows a lateral view

of the spinal cord at 2.5 dpf. Intense GFP signal was observed in p0/V0 domain. In

addition, many GFP positive cells that were located in a more dorsal region were

observed. All of these cells appeared to be postmitotic neurons, as inferred by their

circular shapes. These results suggest that after being generated in the V0 domain, some

of the postmitotic V0 neurons migrated in a dorsal direction. It should be noted that the

presence of these dorsally-located GFP positive cells was not due to ectopic expression

of *gfp* in the transgenic fish, because *gfp* mRNA expression was confined to p0/V0

domain throughout the stages we examined (from 24 hpf to 2.5 dpf; data not shown).

Figure 3E shows a lateral view of the spinal cord at 3.5 dpf. By this stage, a large

number of V0 postmitotic neurons were generated. Many GFP-labeled axons that

crossed the bottom of the spinal cord (arrows in Fig. 3E) are discernible, indicating that

V0 neurons are predominantly commissural neurons.

Neurotransmitter properties of V0 neurons

Next, I investigated the neurotransmitter properties of V0 neurons. In the spinal cord,

glutamate is a major excitatory neurotransmitter, and glycine is a major inhibitory

neurotransmitter. I examined the neurotransmitter properties of neurons using transgenic fish. For this purpose, I generated Tg[*vglut2a*:loxP-DsRed-loxp-GFP] transgenic fish (Fig. 2D) Because the fish expressed just DsRed without applying Cre recombinase, the line will be referred to as Tg[*vglut2a*:DsRed] in this section. *vglut2a* (vesicular glutamate transporter 2a) is known to be expressed in many glutamatergic neurons in zebrafish (Higashijima et al., 2004a), and thus, the transgenic fish could be used as a marker strain for glutamatergic neurons. For glycinergic neurons, I used Tg[*glyt2*:GFP] transgenic fish (McLean et al., 2007). To reveal *dbx*-labeled glycinergic neurons in this strain, I generated Tg[*dbx1b*:loxP-DsRed-loxp-GFP] (Fig. 2B; referred to as Tg[*dbx1b*:DsRed] hereafter).

Figures 4A1-3 show cross sections of compound transgenic fish of Tg[*dbx1b*:GFP] and Tg[*vglut2a*:DsRed] at 2.5 dpf. Cells dually positive for GFP and DsRed (arrowheads in Figs. 4A1-3) were present, indicating that glutamatergic neurons are included among the V0 population. Figures 4B1-3 show cross sections of compound transgenic fish of Tg[*dbx1b*:DsRed] and Tg[*glyt2*:GFP] at 2.5 dpf. Again, cells dually positive for GFP and DsRed (arrowheads in Figs. 4B1-3) were present, indicating that glycinergic neurons are included among the V0 population. I also examined whether or not GABAergic neurons were included among the V0 neurons. For this, Tg[*dbx1b*:GFP] fish at 2.5 dpf were counterstained with an anti-GAD65/67 antibody. As shown in Figures 4C1-3, cells dually positive for GFP and GAD were present. Together, my results indicated that glutamatergic, glycinergic and GABergic neurons are included among V0 neurons. This is consistent with the situation in amniotes: in mice and birds, both excitatory (glutamatergic) and inhibitory (GABAergic and glycinergic) neurons are generated from p0 progenitors (Lanuza et al., 2004).

In amniotes, p0 progenitors have been shown to produce astrocytes in the later phase of neurogenesis (Fogarty et al., 2005). I asked whether astrocytes were produced from *dbx1b*-expressing progenitors. Figures 4D1 shows a cross section of the spinal cord at 5.5 dpf. Cell bodies that were clearly positive for GFP were only recognized in the medial region of the spinal cord (arrowhead in Fig. 4D1). Laterally-extending processes originating from these cells were observed (arrows in Fig. 4D1). These are likely to be astrocytes, because the GFP positive cell bodies and processes were also positive for dTomato signal in Tg[*gfap*:dTomato] (Figs. 4D1-3. GFAP (glial fibrillary acidic protein) is an intermediate filament protein that is expressed in astrocytes. Thus, as in mice, p0 progenitors produce astrocytes after producing V0 neurons. At this later stage, recognition of V0 neurons by GFP expression became difficult because of decreases in GFP expression levels in postmitotic V0 neurons.

Morphology of V0 glutamatergic neurons

I next examined the morphology of V0 neurons. In Tg[*dbx1b*:GFP] transgenic fish, GFP expression persisted in postmitotic V0 neurons. However, the expression level of GFP gradually decreased over time, resulting in faint expression of GFP in V0 postmitotic neurons at 4-5 dpf (e.g., see Fig. 4D1 for 5.5 dpf). Therefore, I decided to utilize Cre/loxP recombination system to label postmitotic V0 neurons. I generated Tg[*dbx1b*:Cre] transgenic fish (Fig. 2C). For the promoters of the flox constructs, I used vglut2a (this section) and glyt2 (later section).

When Tg[*dbx1b*:Cre] transgenic fish were crossed to Tg[*vglut2a*:loxP-DsRed-loxp-GFP], Cre-mediated recombination occurred in

dbx1b:Cre-expressing cells, resulting in GFP expression in postmitotic V0 excitatory neurons. Figure 5A shows an example of such compound transgenic fish at 2.5 dpf. This method enabled me to see post-mitotic V0 glutamatergic neurons at 4-5 dpf. However, there were many labeled neurons, and thus, it was difficult to perform fine morphological analyses. To overcome this, I combined the Cre/loxP system with a transient expression system. In a transient expression system in which DNA-injected fish themselves are analyzed, exogenously-introduced DNA is retained in a random subset of cells, resulting in mosaic expression of the foreign gene. Thus, in the scheme shown in Figure 5, a small number of glutamatergic neurons that derived from *dbx1b*:Cre expressing cells express GFP. An example is shown in Figure 5B (left panel).

I looked for fish that had isolated GFP expressing cells, and performed detailed morphological analyses using 5 dpf larvae. More than 100 cells were analyzed. The primary process which is long and extended from soma is considered as an axon, the others are considered as dendrites. The fundamental feature that could apply to all the GFP-labeled cells was their commissural nature. The axons of all the neurons first extended ventrally, crossed the midline at the bottom of the spinal cord, and then projected longitudinally along the contralateral side of the spinal cord. The commissural nature of the axons is apparent in the depth-code view shown in Figure 5B (right panel). Besides their commissural nature, V0 glutamatergic neurons were not morphologically homogenous. I categorized the neurons based on (1) their axonal trajectory on the contralateral side, and (2) the distinctive characteristics of their dendrites.

Based on the axonal trajectories, V0 glutamatergic neurons were categorized into three types: commissural ascending neurons (Figs. 6A and B), commissural bifurcating neurons (Fig. 6C) and commissural descending neurons (Fig. 6D and E). In some cases, commissural ascending neurons had a thin and short descending axonal branch (Fig. 6A). Commissural ascending neurons were further subdivided into two types based on their dendritic morphology. One type of neuron had multipolar cell bodies with longitudinally extending dendrites in both rostral and caudal directions (Figs 6A and F). I named these neurons V0-eMA (V0, excitatory, multipolar, and ascending) neurons. In some cases, thin, short descending axonal branches were present (Fig. 6A). The other type of neuron had unipolar cell bodies (Figs. 6B and G). Short dendrites came off from the ventrally-extending primary process (Fig. 6G). I named these neurons V0-eUA (V0, excitatory, unipolar, and ascending) neurons. Neurons belonging to both of the classes were located in a relatively dorsal region of the spinal cord.

Figure 6C shows an example of commissural bifurcating neurons. Neurons belonging to this class had oval cell bodies with their major axis in the dorso-ventral direction. Cell bodies were located about midway along the dorso-ventral axis of the spinal cord. Dendrites came from the primary process (Fig. 6H; in this stacked figure, a dorsally-extending process seems to come off from the soma, but it actually came off from the ventrally-extending primary process). On the contralteral side, the axon bifurcated, and projected in rostral and caudal directions. Along the way, the axon sent off many prominent collaterals in the dorsal direction. These prominent collaterals were densely distributed in the proximal region of the axons (within a few segments). In the

distal region of the axon, the density of the collaterals sharply drops. I named neurons having these morphological properties V0-eB (V0, excitatory, and bifurcating) neurons.

Two types of descending commissural neurons were identified with one type being multipolar (Fig. 6D and I) and the other type being unipolar (Fig. 6E and J). I named these neurons V0-eMD (V0, excitatory, multipolar, and descending) neurons and V0-eUD (V0, excitatory, unipolar and descending) neurons, respectively. Both types of neurons likely correspond to those that were previously identified in backfilling studies (Bernhardt et al., 1990; Hale et al., 2001). In these previous studies, neurons of the former and the latter type were named multipolar commissural descending (MCoD) neurons and unipolar commissural descending (UCoD) neurons, respectively. The V0-eMD and V0-eUD neurons fulfilled all the hallmarks for the identification of MCoD and UCoD neurons. For V0-eMDs/MCoDs, these include: (1) irregularly shaped cell bodies, (2) elaborate dendritic arbors, which often arise from the rostral and caudal margins of the soma, and (3) superficially located cell bodies in relatively ventral spinal cord (Fig. 6I). For V0-eUDs/UCoDs, the features include: (1) unipolar, mediolaterally elongate cell bodies, (2) medially located somata midway along the dorso-ventral axis, and (3) a laterally-extending primary process from which dendrites come off (Figs. 6J and K).

Using the preparations in which GFP-labeled cells were well isolated, I examined the axonal length of the neuron of each class. As with the morphological analyses described above, 5 dpf larvae were used. Data from two types of ascending neuron (V0-eMA and V0-eUA) were pooled, as there appeared no difference in axonal length in these two populations. Similarly, two types of descending neuron (V0-eMDs

and V0-eUDs) were pooled. Figure 7 shows the summary of the analyses. The axons of

the ascending neurons (V0-eMA and V0-eUA) usually extended near or into the

hindbrain (Fig. 7, top). The average length of the axons was 11.7 ($\pm$ 4.1) segments. The

axons of the bifurcating neurons (V0-eB) extended 1-8 body segments in rostral and

caudal directions (Fig. 7, middle). The average length of the total (rostral and caudal)

axons was 8.9 ($\pm$ 4.0) segments. The axons of the descending neurons (V0-eMD and

V0-eUD) tended to be long, often extending near the tail (Fig. 7, bottom). The average

length of the axons was 15.4 ($\pm$ 3.7) segments.

Morphology of V0 glycinergic neurons

Next, I examined the morphology of V0 glycinergic neurons. The

glyt2:loxP-DsRed-loxP-GFP DNA construct was injected into Tg[*dbx1b*:Cre] embryos

at the one- to four-cell stage. This produced a small number of GFP –labeled glycinergic

neurons that derived from *dbx1b*:Cre-expressing cells. I examined more than 50 neurons.

Compared to the situation in V0 glutamatergic neurons, the morphology of V0

glycinergic neurons appeared to be more homogeneous. Two representative examples

are shown in Figures 8A-D. The cell bodies of *gfp*-positive neurons that were mainly

located in the dorsal half of the spinal cord were predominantly unipolar. The dendritic

processes that arose from the ventrally-extending primary process radiated superficially

toward the surface of the spinal cord. The primary process, which became an axon,

crossed the midline at the bottom of the spinal cord, and projected to the contralateral

side. Then, the axons bifurcated with one axon ascending and the other descending

(Figures. 8A and B). The branching points on the opposite side were near the ventral

edge of the spinal cord. All the neurons except for one had bifurcating axons: one neuron had only a descending axon. Axons on the contralateral side possessed swellings or collaterals (Figs. 8A and B)

Neurons that have similar morphological features to the neurons described above have been described in previous studies (Hale et al., 2001; Higashijima et al., 2004b), and were named CoBL (commissural bifurcating longitudinal) neurons. However, neurons that could be called CoBLs might represent a broader population, not just V0 glycinergic neurons. Indeed, my preliminary analyses suggest that commissural bifurcating neurons are also generated from progenitors that are located in a more dorsal location than p0 domain (data not shown). For this reason, I use the term, V0-iB to refer to CoBLs that derive from V0 domain (i represents "inhibitory").

I quantified the axonal length of V0-iBs (Figure 8E). The axons usually extended to 1-5 body segments in rostral and caudal directions. The average of the axonal length (total of ascending and descending) was 4.9 ($\pm$ 2.4) segments. This value is much smaller than that of any class of V0 commissural excitatory neuron (Fig. 7).

Physiological analyses of glycinergic V0 neurons

I then performed electrophysiological analyses of V0 neurons to assess their functional role in spinal neuronal circuitry. Because glycinergic V0 neurons were morphologically more homogeneous than V0 glutamatergic neurons, glycinergic V0 neurons were chosen as an initial target. My hypothesis for the role of V0 glycinergic neurons was that they would be involved in reciprocal inhibition of body movements during

swimming, i.e., V0-iBs would be involved in the regulation of left and right alteration during motor activity. This hypothesis came from previous studies in frog tadpoles and adult lampreys: in these animals, there exist commissural glycinergic neurons that provide inhibition to the contralateral side. These neurons have been shown to fire mostly in phase with nearby motoneurons during swimming, consistent with their likely role in reciprocal inhibition (Buchanan, 1982; Buchanan and Cohen, 1982; Roberts et al., 2008). Because V0-iBs that I identified are alike for these neurons in their morphologies, I expected that V0-iBs would play a similar role. If so, then, they should fire during swimming mostly in phase with nearby motoneurons.

For the identification of V0-CoBLs in electrophysiological experiments, I took the same approach described above; combination of transient expression with Cre/loxP. In addition, I generated Tg[*glyt2*:loxP-DsRed-loxP-GFP] stable transgenic fish, and thus, compound transgenic fish for Tg[*glyt2*:loxP-DsRed-loxP-GFP] and Tg[*dbx1b*:Cre] were also used in later experiments. Fish that had GFP labeling in V0-iBs at 3-4 dpf were immobilized with a neuromuscular junction blocker (see Materials and Methods). Then, I performed targeted patch electrophysiological recordings from GFP-labeled neurons, and simultaneously recorded from peripheral motor nerves (ventral root; VR) to monitor the motor pattern during fictive locomotion (Fig. 9A). Because the sites of the VR and patch recordings were several segments apart, I corrected for the timing of the VR data so that it would represent motor activity in the same segment as the patch recordings (see, Materials and Methods). Figures 9B-D show three representative examples of electrophysiological recordings from V0-iBs. As expected, the rhythmic depolarizations of the membrane potential in the V0-iBs during swimming occurred mostly in phase with VR activity. Firing of V0-iBs was also observed during depolarizing phases. The

probability of firing in V0-iBs in each cycle differed from cell to cell. Some fired with high probability (Fig. 9B). Others fired with lower probability (Figs. 9C and D). In these cases, firing tended to occur near the beginning of the swimming episode (Figs. 9C and D).

The phase relationship between spikes of V0-iBs and VR activity was further quantified, as shown in Figures 9E. The phase (Φ) of each spike was calculated relative to the corresponding burst event, and the value was plotted on a circle (Fig. 9F). The shaded area represents the mean of the VR activity, while the arrow ($\bar{\Phi}$) in the circle represents the mean of the plotted spots (spikes of the V0-iB). For each cell, this analysis was performed using at least 20 spikes (typically, > 40). Figure 9G shows a representative example of a V0-iB neuron. In Figure 9H, the results of the 9 cells are shown. The majority of the arrows are located within the shaded area with none being located in the bottom half of the circle. Thus, this quantitative analysis further supports the notion that V0-iBs preferentially fired in phase with the nearby VR activity

DISCUSSION

In this study, I performed a detailed morphological analysis of V0 neurons in larval zebrafish using transgenic fish lines that express fluorescent proteins in *dbx1*-expressing cells and/or their progeny. I found the following: (1) all of the V0 neurons are commissural and are composed of both excitatory and inhibitory neurons. (2) V0 excitatory neurons are morphologically heterozygous, whereas V0 inhibitory neurons are relatively homogeneous. For V0 inhibitory neurons, I performed electrophysiological recordings, and found that V0 inhibitory neurons fire broadly in phase with nearby motoneurons during fictive swimming. This suggests that V0 inhibitory neurons are involved in reciprocal inhibition of body movements during swimming.

Methodological comments

I employed several methods to visualize *dbx1b*-expressing cells and/or their progeny. Tg[*dbx1b*:GFP] and Tg[*dbx1b*:DsRed] were first used to analyze the overall distribution of p0/V0 cells. The transgenic fish, however, were not appropriate to analyze post-mitotic V0 neurons at later stages (4-5 dpf) due to a decrease in the fluorescence levels of these cells. Thus, I used the Cre/loxP system, which is better suited for labeling post-mitotic neurons. For flox strains against Tg[*dbx1b*:Cre], I generated Tg[*vglut2a*:loxP-DsRed-loxP-GFP] and Tg[*glyt2*:loxP-DsRed-loxP-GFP]. Utilization of *vglut2a* and *glyt2* promoters, instead of a pan-neuronal promoter, was advantageous,

because it enabled the visualization of V0 excitatory and V0 inhibitory neurons separately. A caveat of this method is that GABAergic V0 neurons cannot be visualized. I was not overly concerned about this for the following reasons. First, GABAergic inhibition does not appear to play a critical role in zebrafish spinal locomotor circuitry (Ali et al., 2000; Buss and Drapeau, 2001). Second, in the spinal cord and brain stem, many inhibitory neurons initially use GABA as neurotransmitter, but then switch their transmitter phenotype to become glycinergic (Nabekura et al., 2004). Therefore, the GAD-positive V0 neurons I observed (Fig. 4C) are likely early versions as the ones that eventually express glycine.

In addition to the usage of compound transgenic fish for the Cre and flox lines, I used the combination of Cre/loxP and transient expression systems to label a small number of V0 neurons for fine morphological analysis. This is one of the advantages of the zebrafish preparation in which transient expression and screening of labeled fish can be achieved with relative ease. I have described several classes of V0 neurons. Some of the neurons were first identified in the present study (eg, V0-iB), and others were among those that have been described in the previous studies using back-filling with fluorescent tracers (eg, V0-eMD/MCoD; (Hale et al., 2001; Higashijima et al., 2004b)). Even for the latter cases, the present study has succeeded in providing a finer resolution of the morphology of these neurons, and most importantly, I have done so for the entire V0 population, not just a subset that can be reliably labeled by backfilling. Thus, the method employed here is powerful, and should be useful for investigating neurons deriving from other domains.

V0 neurons are commissural and composed of both excitatory and inhibitory neurons

In mice, p0 progenitors give rise to two major groups of neurons; commissural excitatory neurons and commissural inhibitory neurons (Pierani et al., 2001). Here, I showed that the situation is the same in zebrafish. This provides another example that basic features of neurons that derive from regions expressing a particular transcription factor are conserved across vertebrate species (Saueressig et al., 1999; Higashijima et al., 2004c; Sapir et al., 2004; Kimura et al., 2006; Crone et al., 2008; Crone et al., 2009). Perhaps, these basic features were already present in ancient vertebrates, and have been preserved in each lineage of vertebrate species.

V0 inhibitory neurons

In aquatic vertebrates that use undulatory body movements for propulsion, one of the basic features of locomotion is alternating activity across the left and right side of the body. For this to be achieved, reciprocal inhibition of neural activity across the left and right side of the spinal cord has been postulated to play an important role. In frog tadpoles and adult lamprey, researchers have found neurons that are involved in this task. The neurons identified (hereafter, called reciprocal inhibition neurons) have the following characteristics: (1) they have commissural axons; (2) they use glycine as a neurotransmitter; and (3) they fire in phase with nearby motoneurons to provide mid-cycle inhibition onto contralateral neurons. The V0-iB neurons identified in this study fulfill many of these characteristics: V0-iB neurons are commissural inhibitory neurons and fire broadly in phase with nearby VR activity. Thus, my results strongly

suggest that V0-iB neurons are involved in the reciprocal inhibition of body movements during swimming in zebrafish. Consistent with this view is the relative shortness of V0-iB axons. With this configuration, the inhibitory effects by V0-iB neurons are restricted to a relatively narrow region of the body: during swimming the region opposite to the active region needs to be inhibited. What is lacking in the current study is the demonstration of the postsynaptic targets of V0-iB neurons. In tadpoles and lamprey, motoneurons as well as premotor neurons, including contralateral reciprocal inhibition neurons, have been shown to be the postsynaptic targets of reciprocal inhibition neurons (Roberts et al., 2008). This circuitry is presumed to be the kernel of left-right alteration during swimming. The basic circuitry for swimming is likely to be similar in larval zebrafish, and thus, I predict that V0-iB neurons make synaptic connection onto motoneurons and premotor interneurons, including their contralateral counterparts.

In my recordings, the probability of firing in V0-iB neurons differs from cell to cell. This might be related to recruitment order among V0-iB neurons: some are active during slow swimming (lower frequency) and others are recruited when swimming gets faster (higher frequency). In the case of ipsilaterally-projecting premotor excitatory neurons (neurons marked by the transcription factor Chx10), neurons that are born early during development tend to be involved in faster movements (Kimura et al., 2006; McLean et al., 2007; McLean et al., 2008). It will be interesting to see whether this could also apply to V0-iB neurons.

Do V0-iBs represent all of the reciprocal inhibition neurons? Although more studies are needed to address this, the current available data suggests that this is not the

case. There are commissural glycinergic neurons whose morphologies differ considerably from V0-iBs. One of the cell types is the so called CoSA (commissural secondary ascending) neuron, whose axon primarily ascends (Higashijima et al., 2004b). Liao and Fetcho (Liao and Fetcho, 2008) reported that CoSAs fire during swimming, apparently in phase with nearby VR activity. This suggests that CoSAs are involved in reciprocal inhibition as well. Currently, the developmental origin of CoSAs is unknown. Systematic investigations of neurons that derive from other domains will answer this question.

The study in Dbx1 mutant mice suggest that V0 inhibitory neurons in mammals play an important role in coordinating movements across left and right sides of the body (Lanuza et al., 2004). Because the mutant mice die at birth, the in vitro spinal cord preparation was used for their investigation. In normal mice, nerve-activity for the left and right limbs alternates during drug-induced locomotor-like activity. In Dbx1 mutant mice, nerve-activity for the left and right limbs falls into synchrony (Lanuza et al., 2004). The cause of this phenotype was presumed to be an alteration of cell fates in V0 inhibitory neurons. This study, combined with my study in zebrafish infers that the evolutionary conservation of V0 neurons can extend to the functional level: in both mammals and fish, V0 inhibitory neurons appear to play a very important role in the alternation of motor activity across the left and right sides of the body. This is consistent with the view that limb-driven locomotion circuits have been built upon swimming-based locomotion circuits during evolution (Goulding, 2009).

V0 excitatory neurons

V0 excitatory neurons are morphologically heterogeneous. Because V0 excitatory neurons fall into classes with distinct morphologies, I speculate that each type plays a different role in spinal rhythm generation. Currently, functional information for V0 excitatory neurons is only available for V0-eMDs/MCoDs, the neurons that have long descending axons. These neurons are active during slow swimming (Ritter et al., 2001; McLean et al., 2007). McLean et al (McLean et al., 2008) demonstrated that V0-eMDs make monosynaptic excitatory connections onto motoneurons located in the very caudal region of the body. Thus, V0-eMDs are premotor neurons, and are clearly involved in motor control. They make synaptic connections onto far-caudally located neurons, suggesting that the excitatory drive coming from V0-eMDs plays an important role in left-right coordinated movements along the longitudinal axis of the body.

For the remaining V0 excitatory neurons, it is not clear whether they are involved in motor control. However, with the exception of the V0-eMAs, the dendritic processes for the V0-eUAs, V0-eBs and V0-eUDs/UCoDs arborize in a relatively ventral region of the spinal cord, like those of V0-eMDs. The marginal zone in the ventral half of the spinal cord is where motor-related neuronal communication is presumed to occur. This suggests that V0-eUAs, V0-eBs and V0-eUDs may also be involved in motor-control related tasks. If so, the long axons of V0-eUDs and V0-eUAs suggest that they may play roles in left-right coordination along the longitudinal axis of the body during movements, like swimming.

In mammals, there is little information available for deducing the function of V0 excitatory neurons. If neurons that have long axons are included among the V0

population, like in zebrafish, those neurons might play important roles for left-right coordinated movements along the longitudinal axis of spinal cord (e.g., propriospinal interneurons). For example, those neurons could be involved in coordinated movements between the ipsilateral forelimb and the contralateral hindlimb. Investigations of mammalian V0 excitatory neurons will hopefully answer this interesting question.

Developmental issues

From a developmental point of view, it is important to determine how the heterogeneity among V0 neurons is established, as this is related to the general issue of how multiple types of neurons arise from a single domain. For zebrafish V0 neurons, two issues need to be considered: the choice between an excitatory and inhibitory fate, and the establishment of heterogeneity among V0 excitatory neurons. For the choice between excitatory and inhibitory phenotypes, several mechanisms could be conceived: (1) By the expression of a transcription factor(s), the p0 domain might be subdivided into two distinct domains, such as p0-A and p0-B. Then, p0-A, and p0-B might exclusively produce excitatory and inhibitory neurons, respectively. (2) Progenitor cells sometimes migrate across the domain boundary and adjust transcription factor code and cell fate to those of the new environment. This phenomenon, which is called ventricular mixing, is another possibility. (3) Via cell-cell interactions among p0 progenitors (or among post-mitotic V0 neurons), cells might adopt their fates. If the last possibility is the case, the Notch-Delta system might be involved (Mizuguchi et al., 2006; Peng et al., 2007; Kimura et al., 2008). For the establishment of heterogeneity among V0 excitatory neurons, neither a subdivision of the p0 domain nor Notch-Delta mediated cell-cell

interactions are likely explanations, because at least five types of neurons are generated. One interesting possibility is that progenitor cells might change their properties over time, and sequentially generate different types of neurons, as has been seen during *Drosophila* neurogenesis (Doe and Technau, 1993; Matsuzaki, 2000). This possibility is supported by the studies in mouse: astrocytes generated from p0 progenitors are known to be produced during later neurogenesis phase. Whatever the case, the most direct way to attack this important developmental question is to perform lineage analyses.
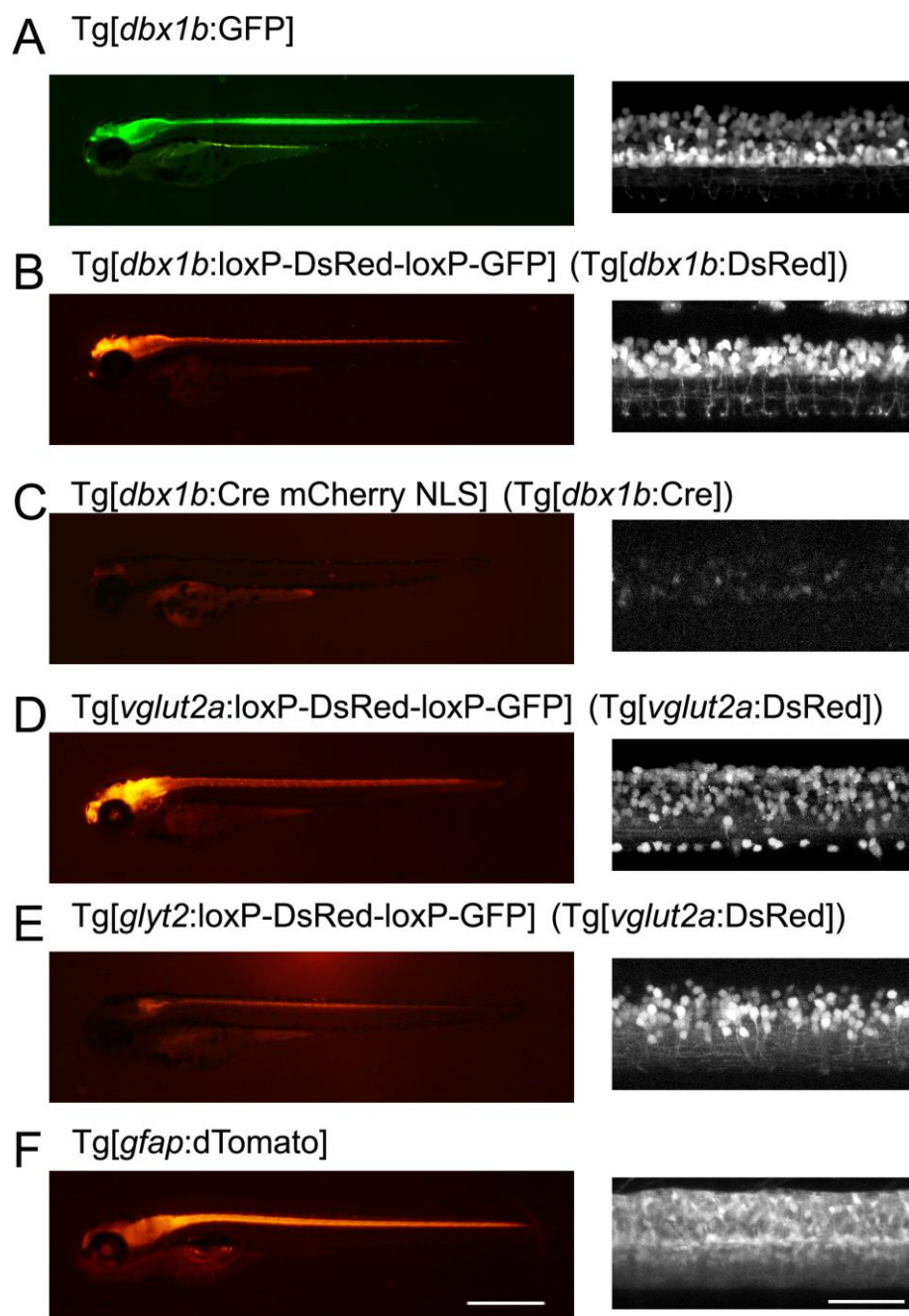
FIGURES and TABLE

Table 1: Constructs and primers used for the generation of the targeting DNA fragment for homologous recombination

| construct	*dbx1b*:GFP
5' prime arm	5'-CCTCTTGGACCCTAATCTACGCAAGTCTCTGCAGTGAGAGAGTGATTTCC-3'
3' prime arm	5'-CTCGGATACATGGCAGGTGGCGCAATAACACTTGGCAACATCATTGCACC-3'
construct	*dbx1b*:loxP-DsRed-loxP-GFP (*dbx1b*:DsRed)
5' prime arm	5'-ATTGTAACGGCATTATGATAATTAACTATAAAGCTACACTGCTTTTATTC-3'
3' prime arm	5'-CTCGGATACATGGCAGGTGGCGCAATAACACTTGGCAACATCATTGCACC-3'
construct	*dbx1b*:Cre (*dbx1b*:Cre-mChreey-NLS)
5' prime arm	5'-ATTGTAACGGCATTATGATAATTAACTATAAAGCTACACTGCTTTTATTC-3'
3' prime arm	5'-CTCGGATACATGGCAGGTGGCGCAATAACACTTGGCAACATCATTGCACC-3'
construct	*vglut2a*:loxP-DsRed-loxP-GFP (*vglut2a*:DsRed)
5' prime arm	5'-TTAACATGCGCATCAAAAACACTATCATTTGCTCCACGTGCAGCATTACT-3'
3' prime arm	5'-TACACGTGCCCCAGTGTCTTCCCCGCAAGTTGCTTCAGCCCCTCTTTGCG-3'
construct	*glyt2*:loxP-DsRed-loxP-GFP (*glyt2*:DsRed)
5' prime arm	5'-TGTTCTTCACAAAAACAACTATTAATCCTTAAAATAAATAATTTCCGTGA-3'
3' prime arm	5'-TTTCTATATCTCCGTGGGAAAGACCGGGTTTGCGTCAGTGCATGGCAAGG-3'

42
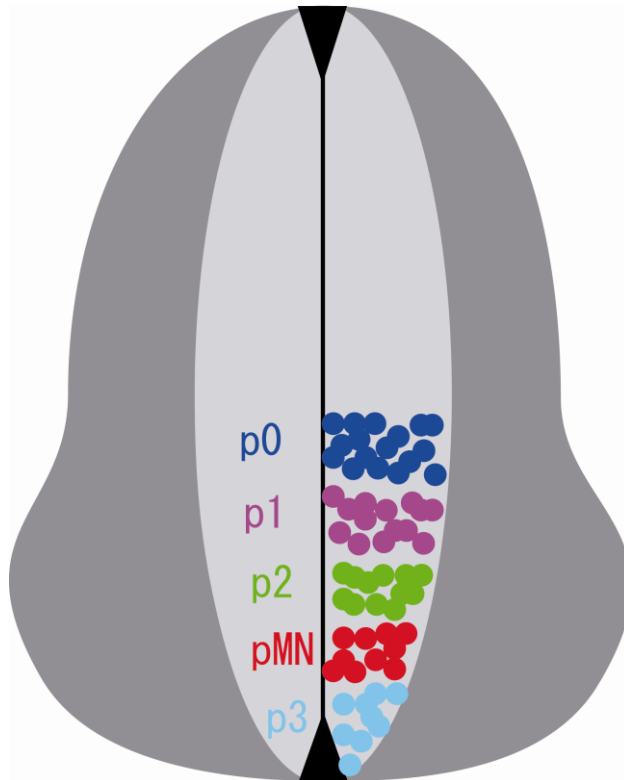
Figure 1. Early development of the spinal cord

Schematic cross-section through the developing spinal cord. Patterning of progenitor pools where progenitor cells expressing the same transcription factors are located in restricted regions of the ventricular zone. These pools are depicted by different colors in the illustration and have been named p0, p1, p2, pMN, and p3 from dorsal to ventral for ventral spinal progenitor populations. Only ventral domains are illustrated in this scheme.

A Tg[*dbx1b*:GFP]

B Tg[*dbx1b*:loxP-DsRed-loxP-GFP] (Tg[*dbx1b*:DsRed])

C Tg[*dbx1b*:Cre mCherry NLS] (Tg[*dbx1b*:Cre])

D Tg[*vglut2a*:loxP-DsRed-loxP-GFP] (Tg[*vglut2a*:DsRed])

E Tg[*glyt2*:loxP-DsRed-loxP-GFP] (Tg[*vglut2a*:DsRed])

F Tg[*gfap*:dTomato]

Figure 2. Transgenic fish generated in this study.

Transgenic fish generated in this study are shown. Pictures of each fish were taken at 2-3 dpf, except for the picture of Tg[gfap:dTomato], which was taken at 5 dpf. Left panels show each transgenic fish larva. Right panels show stacked images of confocal optical sections. lateral view of the spinal cord. **A,** A Tg[*dbx1b*:GFP] transgenic fish at 2 dpf. **B,** A Tg[*dbx1b*:loxP-DsRed-loxP-GFP] (Tg[*dbx1b*:DsRed]) transgenic fish at 2 dpf. **C,** A Tg[*dbx1b*:Cre mCherry NLS] (Tg[*dbx1b*:Cre]) transgenic fish at 2 dpf. **D,** A Tg[*vglut2a*:loxP-DsRed-loxP-GFP] (Tg[*vglut2a*:DsRed]) transgenic fish at 2 dpf. **E,** A Tg[*glyt2*:loxP-DsRed-loxP-GFP] (Tg[*glyt2*:DsRed]) transgenic fish at 2 dpf. **F,** A Tg[*gfap*:TMT] transgenic fish at 2 dpf.   Scale bars; Left, 250 μm; Right, 50 μm
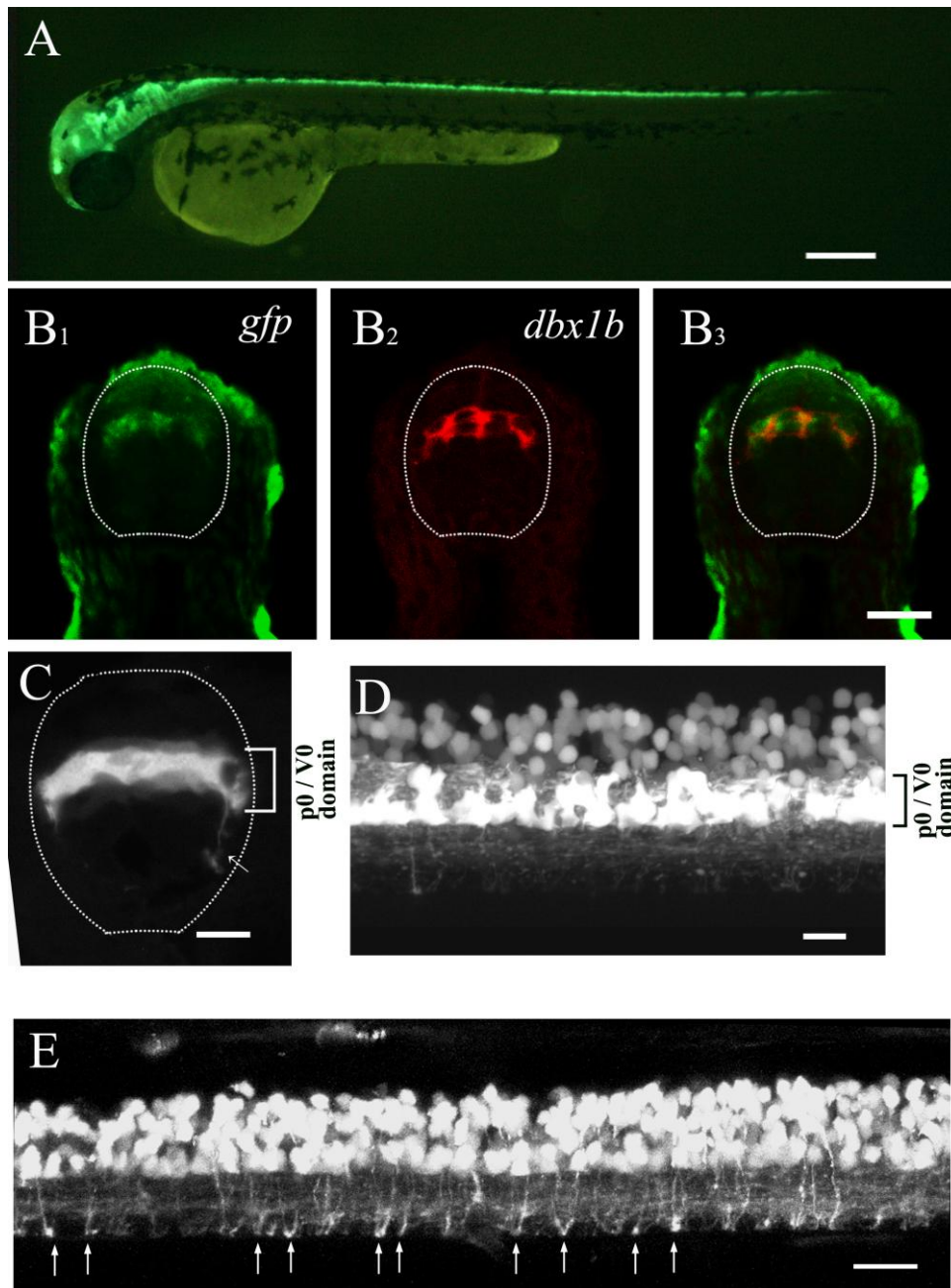
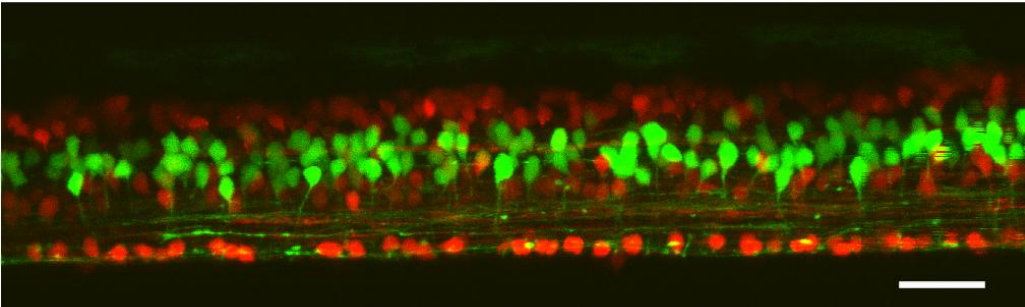**Figure 3. Tg[dbx1b:GFP] transgenic fish.**

A, A Tg[*dbx1b*:GFP] transgenic fish at 2 dpf. **B**, Double in situ hybridization

of *dbx1b* and *gfp* in a Tg[*dbx1b*:GFP] transgenic fish at 32 hpf. Cross section of the

spinal cord. The left panel (B1) shows the staining of *gfp* mRNA, whereas the middle

panel (B2) shows the staining of *dbx1b* mRNA. The right panel (B3) shows the merged

image. The dotted line demarcates the spinal cord. **C**, Cross section of the spinal cord of

a Tg[*dbx1b*:GFP] transgenic fish at 36 hpf. A stacked image of confocal optical sections.

An arrow indicates axons from GFP-expressing neurons. **D**, Lateral view of the spinal

cord of a 2.5-dpf larva. A stacked image of confocal optical sections. **E**, Lateral view of

the spinal cord of a 3.5-dpf larva. A stacked image of confocal optical sections. Scale

bars: **A**, 250μm; **B**, **C, D,** 10 μm; **E**, 50 μm.
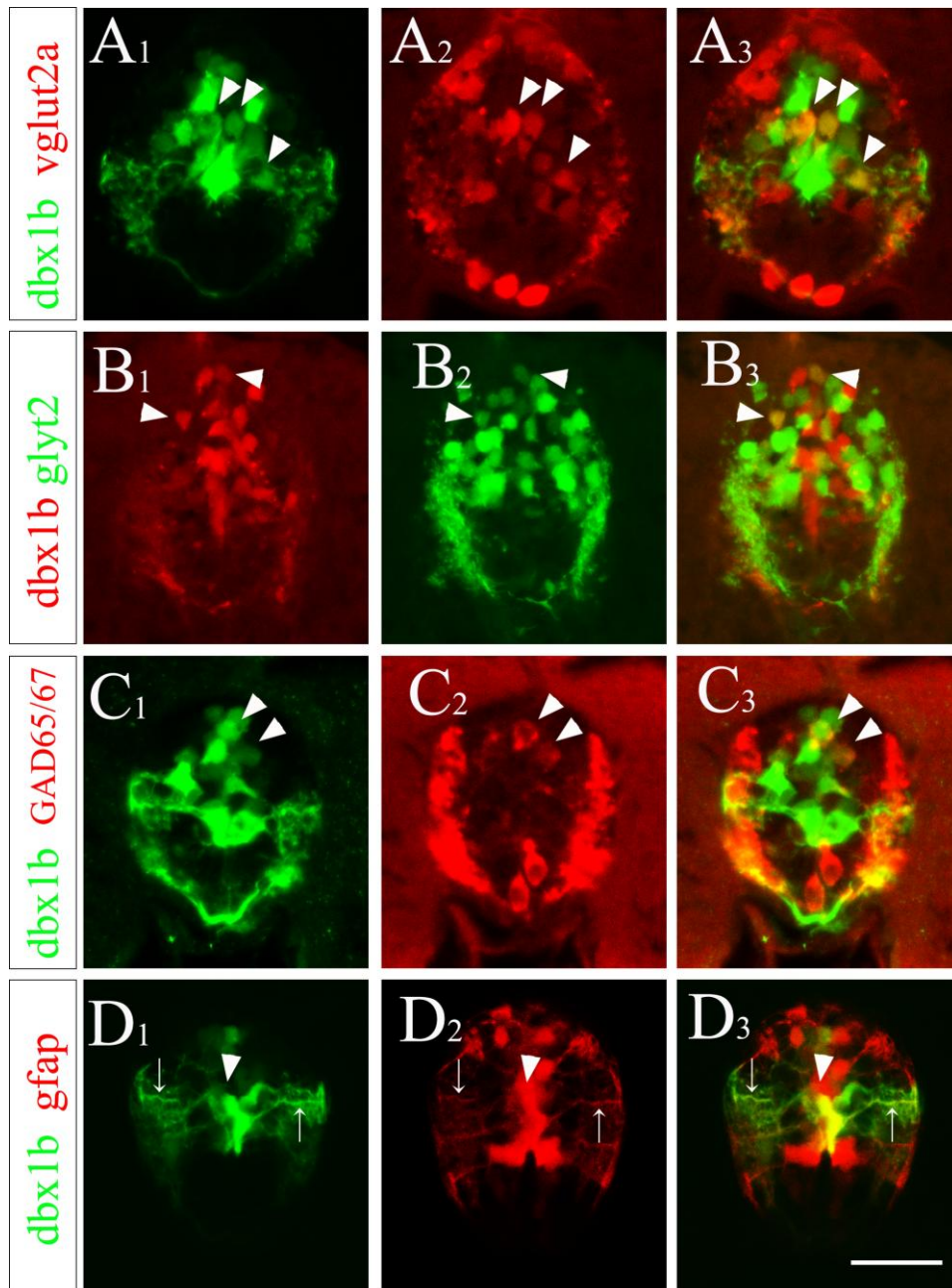
Figure 4. Neurotransmitter properties of spinal V0 neurons.

Cross sections were observed by confocal microscopy. All the pictures are stacked images of confocal optical sections. **A,** Compound transgenic fish of Tg[*dbx1b*:GFP] and Tg[*vglut2a*:DsRed] at 2.5 dpf. Arrowheads indicate cells that are dually positive for GFP and DsRed. **B,** Compound transgenic fish of Tg[*dbx1b*:DsRed] and Tg[*glyt2*:GFP] at 2.5 dpf. Arrowheads indicate cells that are dually positive for GFP and DsRed. **C,** Immunostaining with GAD65/67 in Tg[*dbx1b*:GFP] at 2.5 dpf. Arrowheads indicate cells that are dually positive for GFP and GAD65/67. Staining in the lateral margin is staining of GAD 67, which is expressed axonal terminals. **D,** Compound transgenic fish of Tg[*dbx1b*:GFP] and Tg[*gfap*:DsRed] at 5.5 dpf. An arrowhead indicates cells that are dually positive for GFP and DsRed. Arrows indicate GFP/DsRed-positive fiber-like processes extending outwards toward the pial surface. Scale bar, 20 μm.

A Tg[*dbx1b*:Cre]xTg[*vglut2a*:loxP-DsRed-loxP-GFP]

B

BAC DNA[*vglut2a*:loxP-DsRed-loxP-GFP]

Tg[*dbx1b*:Cre]
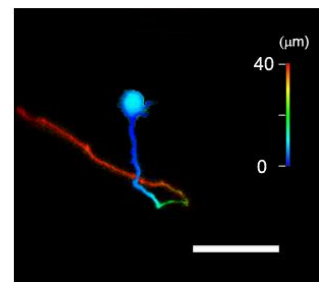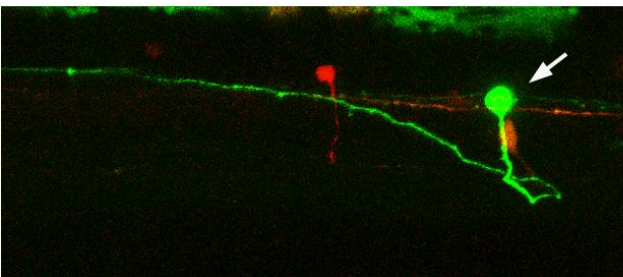
Figure 5. Visualization of glutamatergic V0 neurons.

A, Compound transgenic fish of Tg[*dbx1b*:Cre] and Tg[*vglut2a*:loxP-DsRed-loxP-GFP] at 2.5 dpf. **B, top panel,** A schematic illustration of the experimental design that enabled the visualization of a small number of V0 glutamatergic neurons using the combination of a transient expression and Cre-loxP systems. **B2, bottom left,** An example image obtained in the experiment illustrated above. **B2, bottom right,** Depth-coded view of the image of the cell shown in the left panel (arrow), showing that GFP-labeled axon is projecting to the contralateral side of the spinal cord. Scale bar, 50 µm.
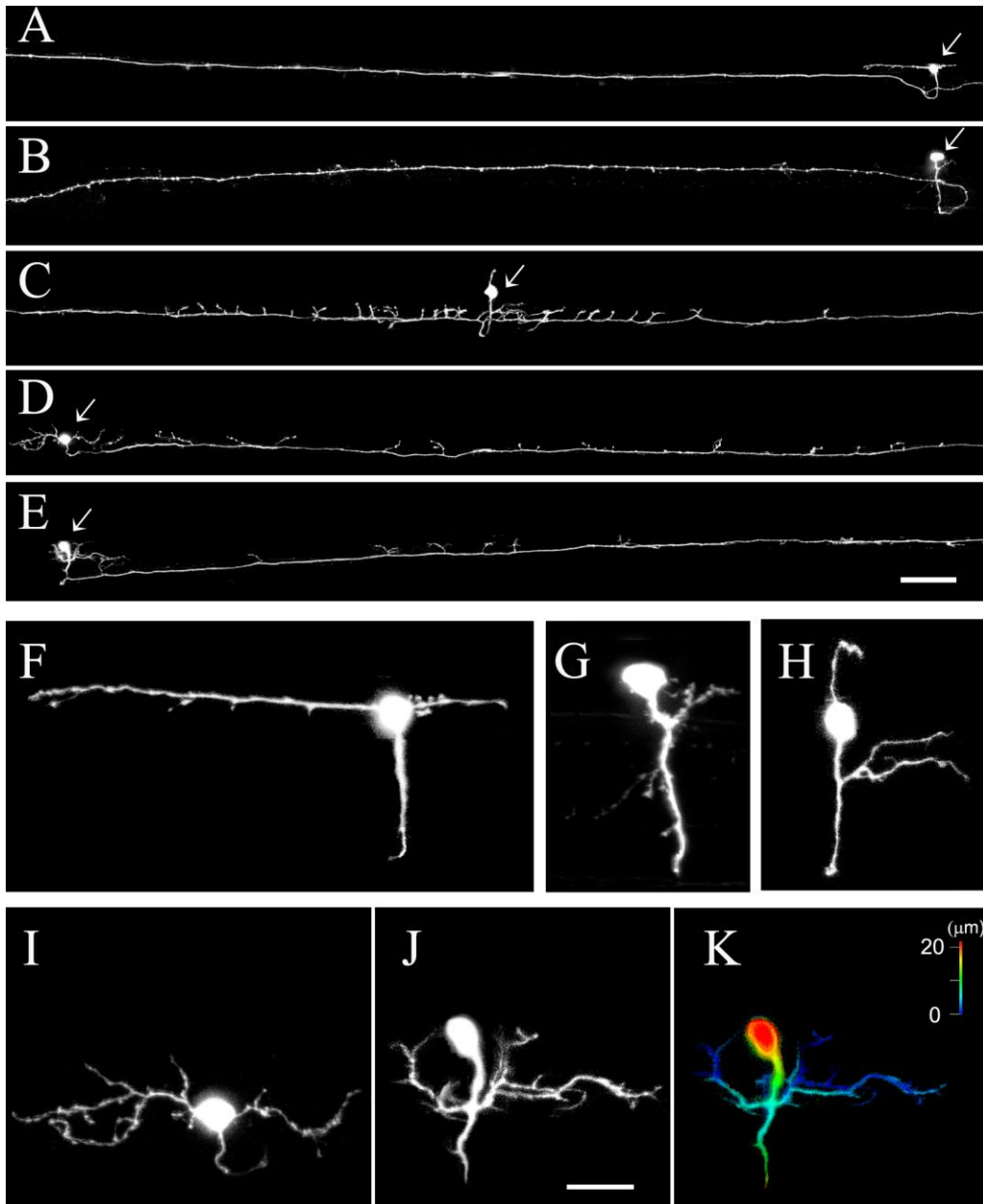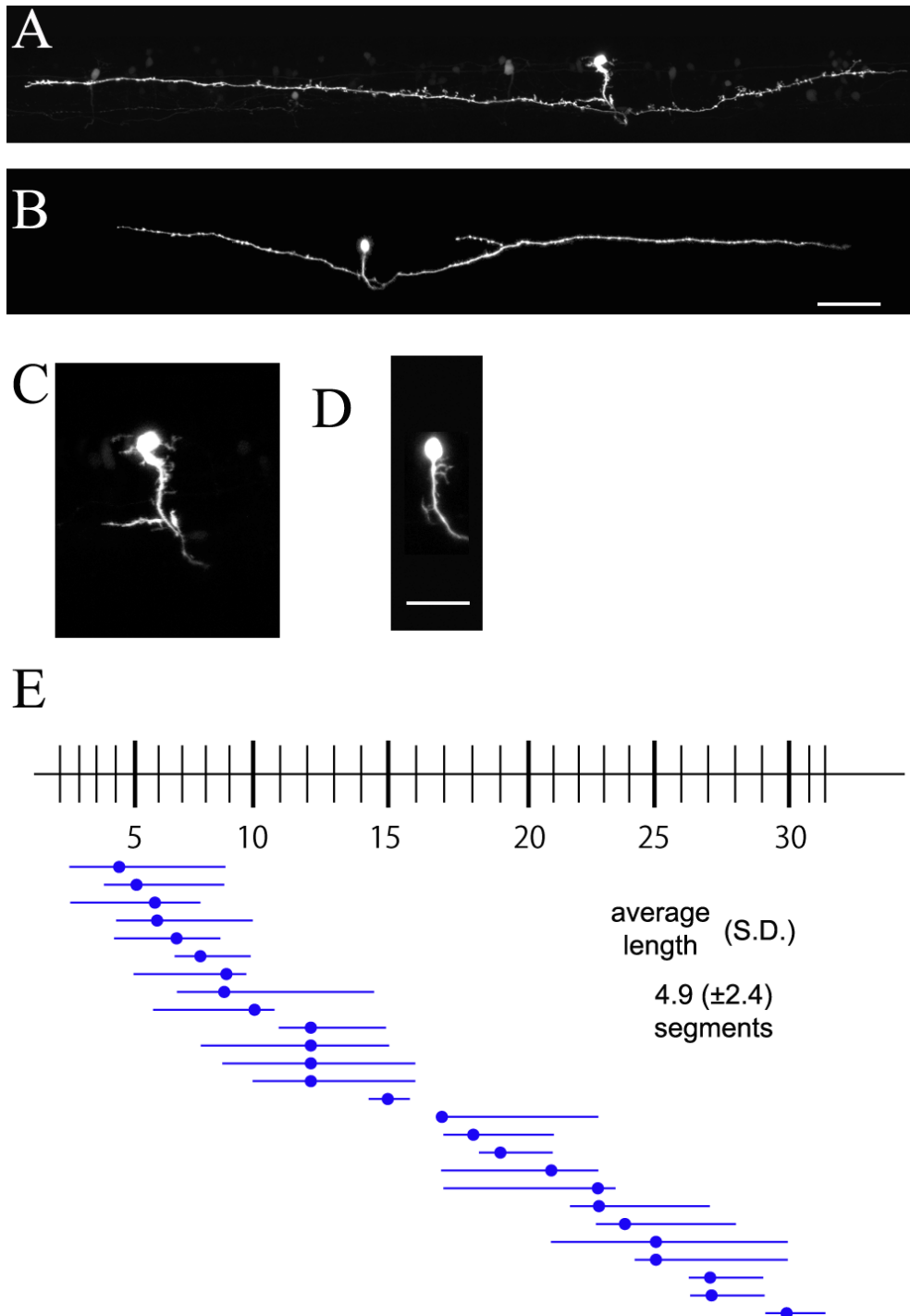
Figure 6. Morphological analysis of GFP-labeled V0 glutamatergic neurons.

Fish that had GFP expression in a small number of V0 glutamatargic neurons were obtained using the experimental scheme shown in Figure 4B. All images (at 5-5.5 dpf) were made from confocal optical sections. Montages were made using the stacked images. **A-E** show the axonal morphologies of GFP-labeled neurons, while **F-J** show the dendritic morphologies of the same neurons shown in A-E. Arrows show cell bodies of each neuron. **A,** An image of a V0-eMA (multipolar ascending) neuron. "e" stands for "excitatory". This cell had a secondary thin axon that projected caudally. **B,** An image of a V0-eUA (unipolar ascending) neuron. **C,** An image of a V0-eB (bifurcating) neuron. **D,** An image of an V0-eMD (multipolar descending) neuron. **E,** An image of a V0-eUD (unipolar descending) neuron. **F,** Dendritic morphology of the V0-eMA neuron shown in **A**. **G,** Dendritic morphology of the V0-eUA neuron shown in **B**. **H,** Dendritic morphology of the V0-eB neuron shown in **C**. **I,** Dendritic morphology of the V0-eMD neuron shown in **D**. **J,** Dendritic morphology of the V0-eUD neuron shown in **E**. **J,** Depth-coded view of the image shown in **J**, showing that the primary process is extending superficially from the medially-located soma. Scale bar, 100 μm for **A-E**; 20 μm for **F-K**.
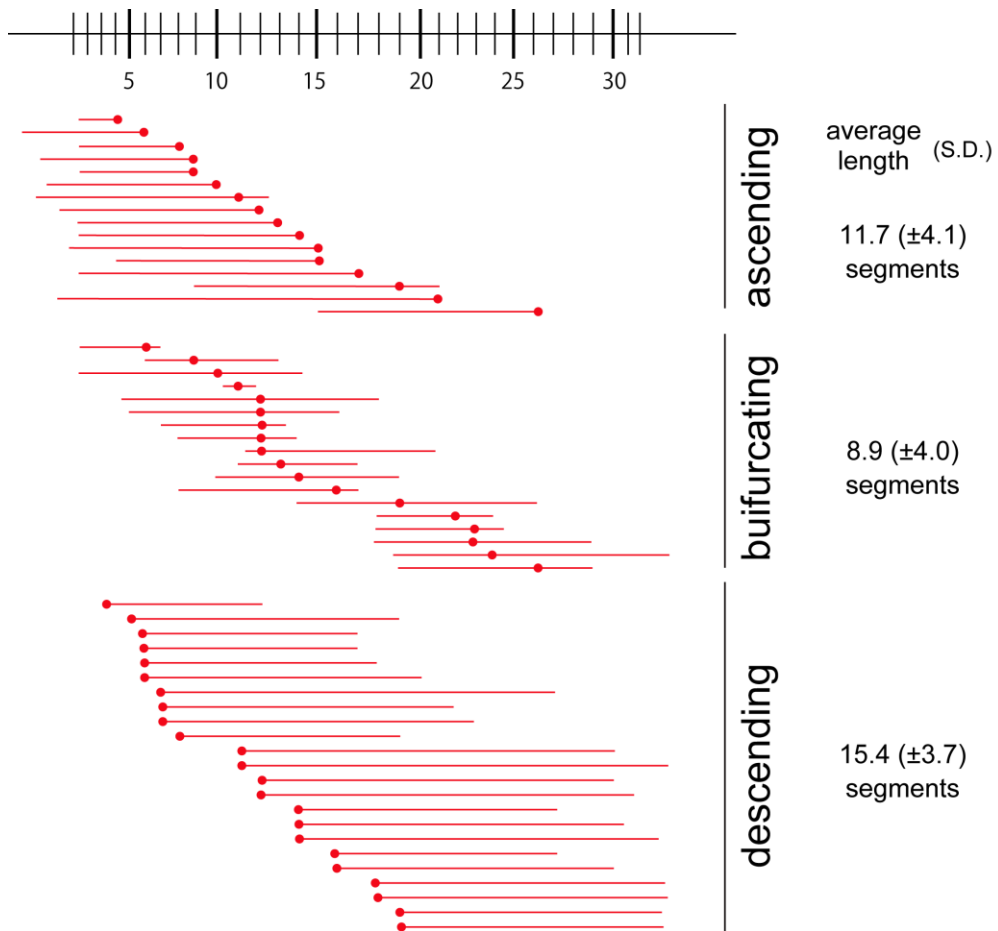
Figure 7. Axonal length of GFP-labeled V0 glutamatergic neurons.

The scale at the top represents body segments. Filled circles indicate the longitudinal positions of the cell body of each neuron. Axonal projections are shown by horizontal lines.

Figure 8. Morphological analysis of GFP-labeled V0 glycinergic neurons.

Fish in which a small number of V0 glycinergic neurons expressed GFP were obtained using the method shown in Figure 5B. DNA of *glyt2*:loxP-DsRed-loxP-GFP was injected into one-cell-stage embryos of Tg[*dbx1b*:Cre]. All images (at 5-5.5 dpf) were made from confocal optical sections. Montages were made using the stacked images. **A** and **B,** Two examples of V0-iB neurons. The complete morphology of each neuron is shown. **C** and **D**, Dendritic morphology of the V0-iB neurons shown in **A** and **B**. The V0-iB neurons are predominantly unipolar. Dendrites come off from the ventrally-extending primary process. **D.** Axonal length of GFP-labeled V0 glycinergic neurons (V0-iBs). The scale at the top represents body segments. Filled circles indicate the longitudinal position of the cell body of each neuron. Axonal projections are shown by horizontal lines. Scale bar **A, B**; 100 μm; **C, D**; 50 μm
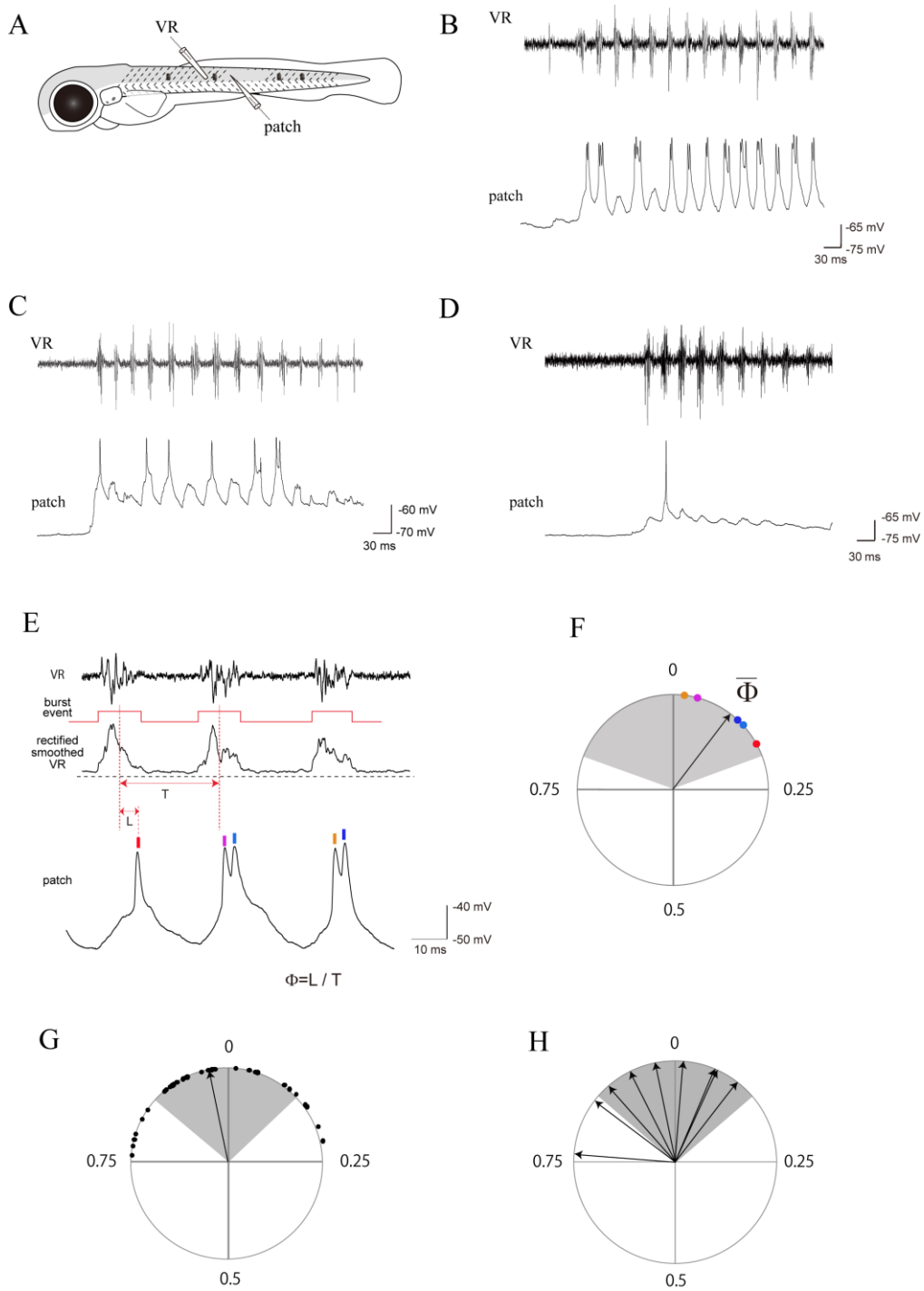
Figure 9. Electrophysiological recordings from V0-iB neurons

A, A schematic illustration of electrophysiological recordings from a V0-iB neuron and VR (ventral root). The black dots represent tungsten holding pins. **B-D,** Three representative examples of the recordings obtained. Each panel represents data obtained from a different V0-iB neuron. **E,** Schematic showing how the phase value (Φ) was calculated. VR recordings were full-wave-rectified and smoothened. Onsets and offsets of the burst were defined whether the rectified signal exceeded the 1.5 times average noise level. The dashed horizontal line shows base line. The cycle time (T) of VR activity started at mid time-point of the burst event and ended at mid time-point of the next burst event. The spike timing in the recorded neurons was defined as the time point of the peak of each action potential. The latency (L) for each spike was measured relative to the beginning of the cycle. Phase (Φ) is calculated as $\Phi = L/T$. **F,** Circular phase-diagram in which the five phase values (red, magenta, light-blue, ocher, and dark-blue spikes in E) have been plotted. The mean phase value ($\overline{\Phi}$) is indicated as the arrow. Shaded area shows burst duration of VR (average of the three burst events). **G,** A representative example of circular phase-diagram in which all the spikes of a V0-iB neuron were analyzed. Shaded area shows burst duration of the VR (average of all the corresponding burst events). The arrow indicates the mean phase value. **H,** Circular phase-diagram in which the mean phase values of the 9 cells analyzed in this study are indicated (arrows). Shaded area shows burst duration of VR.

CHAPTER Ⅱ :

Functional Role of a Specialized Class of Spinal Commissural Inhibitory Neurons during Fast Escapes

SUMMARY

In teleost fish, the Mauthner (M) cell, a large reticulo-spinal neuron in the brainstem, triggers escape behavior. Spinal commissural inhibitory interneurons that are electrotonically excited by the M-axon have been identified, but the behavioral roles of these neurons have not yet been considered. Here, I studied these neurons, named CoLo (commissural local), in larval zebrafish using an enhancer-trap line in which the entire population of CoLos was visualized by GFP. CoLos were present at one cell per hemi-segment. Electrophysiological recordings showed that an M-spike evoked a spike in CoLos via electrotonic transmission, and that CoLos made monosynaptic inhibitory connections onto contralateral primary motoneurons, consistent with the results in adult goldfish. I further showed that CoLos were active only during escapes. I examined the behavioral roles of CoLos by investigating escape behaviors in CoLo-ablated larvae. The results showed that the escape behaviors evoked by sound/vibration stimuli were often impaired with a reduced initial bend of the body, indicating that CoLos play important roles in initiating escapes. I obtained several lines of evidence which strongly suggested that the impaired escapes occurred upon bilateral activation of the M-cells: in normal larvae, CoLo-mediated inhibitory circuits enable animals to perform escapes even in these occasions by silencing the output of the slightly delayed firing of the second M-cell. This study illustrates (1) a clear example of the behavioral role of a specialized class of interneurons and (2) the capacity of the spinal circuits to filter descending commands and thereby produce the appropriate behavior.

INTRODUCTION

Upon sudden stimuli, fish perform an escape, which starts with a rapid bend of the body to one side. Mauthner (M) cells, a bilateral pair of large reticulo-spinal neurons in the brainstem, play an important role in initiating an escape: a single spike in one of the M-cells triggers an escape toward the contralateral side (Nissanov et al., 1990; Eaton et al., 2001; Korn and Faber, 2005). During Mauthner-triggered escapes, motoneurons on the side of the escape bend are activated, whereas those on the opposite side are almost simultaneously inhibited (Yasargil and Diamond, 1968). This suggested the presence of commissural inhibitory neurons that were instantaneously activated by the M-spike via electrical synapses (Diamond, 1971). These interneurons were subsequently identified by electrophysiological studies in goldfish (Fetcho and Faber, 1988), and by electron-microscopic studies in tench (Yasargil and Sandri, 1990).

However, several questions still remain. First, it remains elusive whether these neurons are present in larval fish. Second, the activity of these neurons during a different behavior, such as swimming, has not been clarified. This relates to an important general question, namely, to what extent is interneuron activity shared in different behaviors. Third, and most importantly, the functional roles of these neurons have not been shown. It remains unclear whether the fast inhibition mediated by these neurons plays a critical role in escape behavior.

I have addressed these issues by taking advantage of an enhancer trap line in which the entire population of these interneurons, named CoLo (commissural local), is

visualized by GFP. I show that CoLos are present in the early larval stage at the rate of one cell per hemi-segment, and that CoLos fire specifically at the early phase of escape behavior. I further show that CoLos play a very important role in escape behavior. The present study strongly suggests that co-activation of both of the M-cells occurs upon sound/vibration stimuli, and that CoLo-mediated inhibitory circuits play a pivotal role in allowing animals to perform escapes in these occasions by silencing the output of the slightly delayed firing of the second M-cell. This study provides a compelling case for dedicated spinal interneurons and their behavioral role in the vertebrate spinal cord.

MATERIALS and METHODS

Enhancer trap screening

The Tol2-based enhancer trap construct, T2KHG, was used for establishing enhancer trap lines (Nagayoshi et al., 2008). The T2KHG construct contained the zebrafish hsp70 promoter (Halloran et al., 2000) and the gfp gene. The Tol056 enhancer trap line identified in screening was outcrossed to the wild type for several generations, and was used in experiments as a heterozygous condition.

Electroporation of rhodamine-dextran into single cells

Single-cell labeling with rhodamine-dextran (M.W. 3000; Invitrogen, Carlsbad, CA) by electroporation was performed essentially as described previously (Bhatt et al., 2004).

Antibody and in situ hybridization staining

Antibody and in situ staining were performed as described Chapter1. To detect neuronal connexin (Cx35/36), I used monoclonal anti-Cx35 (MAB3045; Chemicon, Temecula, CA) raised against recombinant fusion protein of perch Cx35 (Pereda et al., 2003). The Cy5-conjugated F(ab')2 fragment of donkey anti-mouse IgG (Jackson ImmunoResearch, West Grove, PA) was used as a secondary antibody.

Neurobiotin staining

Neurobiotin (Vector Laboratories, Burlingame, CA) was loaded into M-cells by a standard patch clamp method (see below). Whole-cell situations were maintained for at least an hour. Positive current pulses were periodically injected through the pipette to facilitate dye-loading. Animals were then fixed overnight with 4% paraformaldehyde in phosphate-buffered saline. After the fixation, samples were first treated with VECTASTAIN Elite ABC kit (Vector Laboratories), and then the signal was visualized using a TSA Kit with Alexa Fluor 647 (Invitrogen) according to the manufacturer's instructions.

Electrophysiology

Patch-clamp and ventral root (VR) recordings were performed as described Chapter1 with some modifications. Recordings were mainly carried out using 3-dpf (3.0-3.6 dpf) and 4-dpf (4.0-4.6 dpf) larvae. For paired recording between Mauthner and CoLo cells, the forebrain region was pierced with tungsten pins such that the head showed near-vertical orientation. The skin covering the hindbrain was removed using a pair of forceps. Then, neuronal tissues overlying the M-cell were removed by a pair of forceps for easier patch electrode access to the M-cell. Because this procedure could have damaged the neuronal circuits surrounding the M-cell, it was used only for paired recording between M-cells and CoLos. CoLos were recorded in the region of segments 11-15. For paired recording between VR and the CoLo neuron, VR recordings were made in the region of segments 6-9 and CoLos recording were made in the region of segments 11-15. Therefore, VR recording sites were always rostral to the patch

electrode recording site. For paired recording between CoLo neurons (bottom side) and primary motoneurons (top side), neuronal tissues overlying CoLos were carefully removed with a pair of forceps for easier access to a patch electrode to the CoLo neuron. Removal of the neuronal tissues was restricted to a small region. Care was taken not to damage the middle to ventral region of the spinal cord, as primary motoneurons to be recorded were located there. Targeting of electrodes to primary motoneurons was made based on their location (middle region of the spinal cord) and their large soma size. As axons of CoLos are short, primary motoneurons located near the recorded CoLos were targeted. After the recordings, identities of primary motoneurons were verified by their torn axons at the lateral edge of the ventral spinal cord.

To elicit fictive locomotion, a stimulation bipolar electrode was placed near the otolith. For the VR and CoLo neuron recordings, the electrode was placed on the bottom side, such that the motor activities associated with escapes would occur on the top side where the VR and CoLo neuron recordings were made. For the CoLo neuron and primary motoneuron recordings, the electrode was placed on the top side, as the recorded CoLo neuron was located on the bottom side. For preparations older than 4 dpf, fictive locomotion was also elicited by changing the illumination intensity. Auditory stimulations, which were used to elicit escapes in behavioral experiments (see below), were not applied in electrophysiological experiments, because auditory stimulations strong enough to elicit escapes would abolish patch recordings.

Pharmacological reagents used were: 10 μM CNQX (Tocris, Bristol, UK), 50 μM D-AP5 (Tocris), 100 μM mecamylamine (Sigma), and 1 μM carbenoxolone (Sigma). Latency of synaptic responses was measured from the peak of the presynaptic

spike to the onset of the responses.

Average spike numbers per escape were calculated using the values of 5 independent escapes. Only those trials in which CoLo spikes occurred were analyzed. In some cells, data were available for less than 5 successful trials. In these cases, average spike numbers from all the successful trials were used for the calculation.

Laser ablation

Laser ablation of Mauthner and CoLo neurons was performed using a MicroPoint pulsed nitrogen laser (Photonic Instruments, St. Charles, IL), with an Axioscope FS upright microscope and a 40x (numerical aperture, 0.8) water immersion objective lens (Zeiss, Jena, Germany). This system allowed the selective targeting of GFP-labeled cells which were ablated by a short series of laser pulses. For M-cell ablation, embryos heterozygous both for Tol-056 and Tol-026 were used. In the Tol-026 enhancer trap line, GFP was expressed in the M-cells and other neurons in the hindbrain. GFP expression in the M-cells was apparent in 30-hpf larvae. I performed M-cell ablation at this stage, as 30-hpf embryos showed less intense pigmentation, which made laser ablation of M-cells easier. Successful ablation was confirmed by the absence of GFP fluorescence in the corresponding region a day after the laser treatment. For the ablation of CoLos, animals at 2.2-2.5 dpf were used. Ablation of CoLos at older stages sometimes resulted in the degeneration of M-axons. As CoLos are connected to the M-axon via gap junctions, the death of a large number of CoLos appeared to have negative effects on the health of the M-axons if the ablation was made in older larvae. Ablation of CoLos at around 2.2-2.5 dpf did not cause this problem. Successive ablation of CoLos was

confirmed by observing the degeneration of the cells under DIC optics.

Behavioral analyses

Larvae at the age of 5 dpf (5.3-5.8 dpf) were used for behavioral analyses. A custom-made sound/vibration stimulation apparatus was used to elicit fast escapes. The apparatus was made of a quadrilateral transparent plastic sheet (75 mm x 180 mm x 2.0 mm height), to which an audio speaker (cone diameter, 75 mm) was attached with screws. A glass Petri dish 45 mm in diameter was tightly attached to the plastic sheet with dental wax. Sponge rubber was attached to the four corners of the bottom of the apparatus. The apparatus was set on a dissecting microscope table using double-sided sticky tape that was applied to the sponge rubber. Water was poured into the dish (approximately 9 mm in height), and a larva was placed in the dish; larvae were examined individually. A stimulation wave (10-msec duration of 500-Hz sine waveform; 5 cycles) was generated by a function generator (FG-281, TEXIO, Tokyo, Japan), amplified by an audio amplifier, and delivered to the speaker. Amplitude of the sound was such that it was around 90 dB when measured at a distance of 15 cm. The acceleration amplitude of the apparatus associated with the stimulus was around 80 m/sec^2 in the vertical dimension. In this condition, larvae showed fast escape responses (latency, < 15 ms) with more than 80% probability. Sequential images of larval locomotion (every 1 msec) were captured with high-speed digital cameras mounted on the dissection microscope. Two types of cameras were used. One was a VCC-1000 (Digimo, Osaka, Japan) with 256 x 256 pixels and the other was a Fastcam Ultima 1024 (Photron, Tokyo, Japan) with 1024 x 512 pixels. The function generator and the

high-speed camera were triggered by a TTL stimulation pulse. Latency was defined as the time between the onset of the sound pulse (arrival of the trigger signal) and the beginning of body movement. Responses with latency shorter than 15 msec were analyzed. Successive trials were separated by at least 2 min. The image field of the camera was set near the center of the dish. Larvae had to stay still in this image field in order to be subjects of the trials. Some larvae seldom came to the center of the dish; for these larvae, I was unable to perform many trials. Consequently, the number of trials performed for each larva was variable. In a minority of cases, larvae started spontaneous movements before the arrival of sound/vibration stimuli. These trials were excluded from the data analyses.

The body shapes of the larvae in the captured images were analyzed with BohBoh (BohBoh Software, Tokyo, Japan), a motion tracker/shape analyzer originally developed for the analysis of flagellar or ciliar beating (Baba and Mogami, 1985; Shiba et al., 2005; Wood et al., 2005). The higher resolution images captured with the Fastcam Ultima 1024 (1024 x 512 pixels) were used for the analyses. The midline of the larval body in each image was semi-automatically traced with quasi-evenly spaced points. In my experiments, magnification of the microscope was set such that the body length corresponded to ~300 pixels in the captured image. Because the software draws approximately one point per pixel, the midline of the body was traced with ~300 drawn points. BohBoh software was used to calculate length and curvature utilizing the drawn points. Images at a time point of 6 msec after the onset of the movement were chosen for curvature analyses. For curvature calculation at each position, drawn points covering ~10% of the body length were used. For example, for calculation of the curvature at mid-body (position 0.5), drawn points covering positions 0.45-0.55 were used.

Calcium imaging

Calcium imaging of M-cells was performed as described previously (O'Malley et al.,
1996; Takahashi et al., 2002; Kohashi and Oda, 2008). Briefly, M-cells were labeled
with a fluorescent Ca^{2+} indicator, Calcium Green dextran (3,000 or 10,000 molecular
weight; Invitrogen) by injecting the dye into the spinal cord of 4-dpf or 5-dpf wild-type
larvae. After the injection, larvae were allowed to recover in 10% Hanks solution for
>5 hr. Larvae at the age of 5.3-5.8 dpf were then mounted on low-melting point agarose
(1.5%; Nacalai Tesque, Kyoto, Japan) in glass-bottomed 35-mm plastic dishes in an
upright position. Larvae were mounted in a near-vertical position, such that the left and
right M-cells were in approximately the same focal plane during the subsequent
observations. The preparation was overlain with Hanks solution (10%) to a water height
of 3-4 mm. The dish was then attached to the sound/vibration stimulation apparatus
(described above) with an orientation such that the head faced toward the audio speaker.
The setting was placed on a BX51WI upright microscope equipped with a FV300
confocal unit (Olympus). A 40x water immersion objective (numerical aperture, 0.8)
was used for the observations. M-cells were illuminated with a 488-nm argon laser and
sequential confocal images (at approximately 400-msec intervals) were taken with a
fully open pinhole. A trigger signal, generated by the confocal scanner, was used to
deliver a time-locked sound/vibration stimulation to the specimen. The stimulation was
applied near the beginning of the 8th frame (2.8 sec after the initiation of the first frame
scan). M-cells were placed near the center of the scanning field in the Y dimension.
Considering the ~400 msec of scanning time per frame, the center of the field in each
frame was scanned approximately 200 msec after the initiation of scanning. I added this
time delay for time scaling. After Ca^{2+} imaging with the sound/vibration stimuli,

d-tubocurarine was added to the solution (final concentration, 0.1 mg/ml) to immobilize the larvae. Then, fluorescence responses associated with antidromic (AD) spikes were examined as described previously (Kohashi and Oda, 2008). For illustration purposes, the images were smoothed to reduce pixel to pixel noise. All quantification, however, was performed on the raw data. Line-scan experiments were performed as described by O'Malley et al. (1996). For the quantification of line-scan experiments, fluorescence intensity change associated with AD spikes (from +100 msec to +250 msec) was averaged, and this averaged value was used for normalization. Smoothing of images was not carried out for the presentation of the line-scan experiment.

RESULTS

Tol-056 enhancer trap line labels a specific class of commissural neurons, CoLos

To search for the transgenic zebrafish in which GFP was expressed in a limited number of CNS neurons, screening was performed from the enhancer trap celloection, which was generated by Takeda laboratory at Tokyo University. The Tol-056 enhancer trap line was identified by this criterion. In the hindbrain, intense GFP expression was observed in the pair of Mauthner (M) cells (Fig. 1A). GFP expression in the M-cell was initiated at around 2.2 dpf, and the intense labeling was maintained for at least 5 dpf. In the spinal cord, GFP fluorescence was observed in the M-axons (Fig. 1B). In addition, two classes of neurons were positive for GFP. One was the Kolmer-Agduhr (KA) neurons located near the bottom of the spinal cord (Roberts and Clarke, 1982; Higashijima et al., 2004b). The other class of neurons, located in a lateral region of the spinal cord (arrows in Fig. 1B), were the focus of the present study. As described below, they are commissural neurons with relatively short axons, leading us to refer to them as CoLo (commissural local) neurons. Several other cells also weakly expressed GFP in the spinal cord. The significant difference in fluorescent intensity, however, made the CoLos clearly apparent.

GFP fluorescence in CoLos became discernable around 40 hpf, and was present for at least 5 dpf. I first examined the location and distribution of CoLos. CoLos were located in a near-fixed position along the dorso-ventral axis (Figs. 1B and D):

approximately 70% of the distance from the bottom of the spinal cord. In the rostral two-thirds of the spinal cord (segments 1-20), CoLos were present at the rate of approximately one CoLo per hemi-segment throughout the stage I examined (Fig. 1D; see also Fig. 7D; note that in Fig. 1B CoLos on both sides of the spinal cord are shown in the confocal stacked image). Furthermore, CoLos tended to be present in a regularly spaced manner at their preferential position within a segment (Fig. 1D). Quantitative analyses using 3.5-dpf larvae showed that the regular distribution pattern was stricter in the rostral region of the spinal cord than in the caudal region (Fig. 1E). In further caudal regions (caudal to the 20th segment), CoLo distribution became more sparse, and ultimately, there were no CoLos near the tail (this was also true in 4.5-dpf larvae).

I examined the neurotransmitter property of CoLos by performing dual in situ hybridization with *gfp* and markers of neurotransmitter properties (Higashijima et al., 2004a). The result, as shown in Figure 1G indicated that CoLos were positive for *glycine transporter2* (*glyt2*), strongly suggesting that CoLos are glycinergic inhibitory neurons.

I then examined the morphology of CoLo neurons by loading rhodamine-dextran or Alexa594 into individual CoLo neurons through electroporation (Bhatt et al., 2004; Kimura et al., 2006) or whole cell recordings, respectively. I have observed more than 100 CoLos, and essentially all of these had the same morphological features throughout the stages examined (2-4 dpf). CoLos had a simple, spherical soma (Figs. 2A, B, C, and D). The somata were located in the most superficial region of the cell layer of the spinal cord. In cross sections, tiny dendritic processes which extended toward the superficial mantle layer were occasionally observed (thin arrow in Fig. 2D).

From the ventral side of the soma, a thin axon came out, and extended ventrally (Figs. 2A, B, C, and D). Upon encountering the M-axon on its dorsal side (fat arrowhead in Fig. 2D), the CoLo axon thickened, and crossed the spinal cord by taking a route dorsal to the M-axon (thick arrow in Fig. 2D). On the contralateral side, the robust CoLo axon mainly descended, and ran along the contralateral M-axon (Fig. 2E), sending off several collaterals (Figs. 2A, B and E). In approximately 70% of CoLos, a relatively short ascending axonal branch, which also ran near the M-axon, was observed (Fig. 2A). The axonal length of the CoLo neurons on the contralateral side (the total length of descending and ascending branches) was short: approximately 1.1-1.2 body segments (Fig. 1F).

CoLos were not observed in the previous survey of glycinergic neurons in larval zebrafish (Higashijima et al., 2004b), presumably due to their short axons which were difficult to reveal by retrograde filling. However, studies for investigating spinal neuronal circuits of M-cells in adult goldfish and tench have revealed a similar morphological type of cells: commissural inhibitory neurons which receive gap junctional inputs from the M-axon (Yasargil and Sandri, 1987; Fetcho and Faber, 1988; Fetcho, 1990; Yasargil and Sandri, 1990). This leads me to speculate that CoLos are zebrafish homologs of these commissural neurons.

Gap junctional inputs from the M-axon drive CoLo spikes

To investigate whether CoLo neurons receive direct inputs from the M-cell, paired recordings were performed between M-cells and the contralateral CoLos (Fig. 3). Recordings were obtained in 8 pairs (6 at 3 dpf and 2 at 4 dpf). In all the pairs,

connections were present. Figure 3B-F shows a representative example. Firing the

M-cell with a somatic current injection produced short latency depolarizing responses in

the CoLo (Fig. 3C). For each pair, the latencies of the responses were very short and

constant (less than 0.1 msec of standard deviation for each pair; Fig. 3D). The

depolarization responses showed very steep rises and sharp peaks (Figs. 3C and D).

Then the membrane voltage slowly returned to the baseline. The presence of sharp

peaks is consistent with the idea that the responses were mediated by electrotonic

synapses. These responses could be either subthreshold electrical PSPs or spikes that

were instantaneously evoked by electrical PSPs; as will be described later, the latter was

the case. The small spike amplitude (ranging 6-16 mV, depending on pairs) was likely

the result of the spike-initiating region being located a relatively long distance from the

recording site at the soma. I speculate that spikes were initiated near the contact site

between the M-axon and the CoLo axon.

To further demonstrate that the spikes were driven by electrotonic synapses,

M-spikes were elicited at a frequency of 100 Hz, at which responses by chemical

synapses would likely be diminished. In the two cases tested, the spikes of CoLos

faithfully followed the M-spikes with the same amplitudes (Fig. 3E). Pharmacology was

also tested. Application of a mixture of CNQX, AP5 and mecamylamine, which would

block chemical excitatory transmission, had no effect on the sharp CoLo responses

(n=2; data not shown). Instead, the responses became negligible after the application of

the gap junction blocker carbenoxolone (Fig. 3F; n=2). These results indicated that

spiking activities of CoLos were driven by the M-cell spikes via electrotonic synapses.

This establishes that CoLos are indeed zebrafish homologs of Mauthner-driven

commissural neurons that were previously identified in adult goldfish and tench.

Gap junctions in CNS electrotonic synapses are known to be mainly composed of neuron-specific connexin (Rash et al., 2001). I investigated whether neuronal connexin was present near the contact site between the M-axon and the CoLo axon by performing immunostaining with a monoclonal antibody against perch Cx35, which is a fish homolog of mammalian Cx36 (O'Brien et al., 1998; Pereda et al., 2003). As expected, intense signals were observed at the contact site between the M-axon and the CoLo axon (Figs. 3G and H). This strongly suggests that these labeled spots were the sites of Mauthner-CoLo electrical synapses. Among all the immuno-stained signals in the spinal cord, the staining intensity of the Mauthner-CoLo synapses was by far the strongest (Fig. 3G).

Next, to examine whether dye-coupling between the M-axon and the CoLo neuron could be observed, neurobiotin, a small molecule which often passes through gap junctions, was loaded into the M-cells by whole-cell recordings. Subsequently, the samples were processed for neurobiotin staining (Figs. 4A and B). In the spinal cord, one of the M-axons was labeled (Fig. 4B, arrow). In addition, CoLos located on the side of the labeled M-axon were labeled (Fig. 4B), indicating that neurobiotin passed through the gap junctions of the Mauthner-CoLo synapses. Segments 8-15 from 6 larvae (3 dpf) was observed, and the results showed that the neurobiotin-labeled cells perfectly overlapped with GFP-labeled CoLos (total number of cells examined, > 45). This indicates that the entire population of CoLos was visualized in the Tol-056 line.

CoLos make monosynaptic inhibitory connections onto contralateral primary motoneurons

In adult goldfish, CoLo-corresponding neurons make monosynaptic inhibitory connections onto contralateral primary motoneurons (Fetcho, 1990). To investigate whether the same connections were present in larval zebrafish, paired recordings between CoLos and contralateral primary motoneurons were performed using 3-dpf larvae.

Recordings were obtained in 4 pairs, and in 3 out of the 4, direct connections were observed (in the one case with no connection, the CoLo axon did not reach the primary motoneuron). A representative example is shown in Figure 5, in which the CoLo neuron and the primary motoneuron were recorded in a current and a voltage clamp mode, respectively. The firing threshold of the CoLo neuron with current injections into the soma was high: more than 50 mV of depolarization at the recording site was usually needed to reach the threshold (Fig. 5C), consistent with the idea that the spike was initiated away from the soma. Upon reaching the threshold, the CoLo showed a single, small amplitude spike (thin arrow in Fig. 5C), which evoked outward current in the primary motoneuron (thick arrow in Fig. 5C). Considering the -50 mV of holding potential in the recordings, this outward current most likely corresponds to an IPSC (the calculated chloride reversal potential of the recording solution was -70 mV). The latencies of the responses were very short (less than 0.2 msec for all 3 pairs), and constant (less than 0.1 msec of standard deviation for each pair) (Fig. 5D). These unusually short latencies for chemical transmissions (usually > 0.5 msec) probably reflect (1) the proximity of the recorded primary motoneuron from the spike-initiation

site of the CoLo (CoLo-Mauthner contact site), and (2) the time-delay of spike detection, caused by back propagation of a spike to the CoLo soma. The short and constant latency responses, in any case, indicate that the connections were monosynaptic. I thus conclude that CoLos make monosynaptic inhibitory connections onto contralateral primary motoneurons. The results also provide supportive evidence that the small-amplitude, sharp responses recorded in the CoLo somata represented spikes.

In the experiment shown in Figure 5, fictive escapes were elicited by applying electrical stimulations around the ear. I expected that these stimulations would activate the auditory nerves, and that this in turn would activate the M-cell. In addition to the M-cell, other reticulo-spinal neurons that are important for initiating escape behavior could also be activated (O'Malley et al., 1996; Kohashi and Oda, 2008). Stimulations were applied to the contralateral side of the recorded CoLo neuron so that that side of the recorded CoLo neuron would initiate escape (Fig. 5A). CoLos often showed several successive spikes upon escapes ("spikes" in Fig. 5E; see the following section for more details). The amplitude of each spike (approximately 10 mV) was comparable to that obtained in paired recordings between M-cells and CoLos. Not all of the CoLo spikes evoked IPSCs in the primary motoneuron. However, as far as the first spikes were concerned, IPSCs were reliably observed (arrows in Figs. 5E and F). Failures of synaptic responses for the subsequent successive spikes were likely due to synaptic fatigues. The IPSCs that CoLo-spikes evoked (arrow in Fig. 5F) corresponded to the earliest synaptic responses that the contralateral primary motoneurons received during escapes. This is consistent with the following idea: the M-spike, which was likely to be the earliest descending input arriving on the side of escape (Casagrand et al., 1999; Eaton et al., 2001), evoked a CoLo spike via an electrotonic synapse with a minimal

delay, and this in turn provided the earliest inhibition onto the contralateral primary motoneuron (Yasargil and Diamond, 1968; Diamond, 1971; Fetcho, 1991). Following these earliest IPSCs, the primary motoneuron received several IPSCs (dots in Figs. 5E and F) that were unrelated to CoLo spikes, suggesting that this later inhibition came from different sources.

I have shown that primary motoneurons are direct synaptic targets of CoLos. Previous studies in adult goldfish have suggested that other neurons are also postsynaptic targets of CoLos. Namely, all the known postsynaptic targets of the M-cell, including CoLos, were shown to receive very fast inhibition upon the contralateral M-spike (Fetcho and Faber, 1988), strongly suggesting that CoLos make inhibitory connections onto all the postsynaptic targets of the M-cell. My anatomical evidence supports the view that contralateral CoLo neurons are also direct synaptic targets of CoLos. As shown in Figure 2E, axonal collaterals of the CoLo were frequently observed near the contact sites of the M-axon and the CoLo axons of its contralateral counterparts (arrowheads in Fig. 2E). This suggests that CoLo neurons inhibit their contralateral counterparts near the Mauthner-CoLo electrical synapses.

CoLos are active only during escapes

To examine firing patterns of CoLos during fictive locomotion, CoLo neuron recordings with recordings from peripheral motor nerves (ventral root, VR; Fig. 6A) were performed. The purpose of the experiments was (1) to examine firing patterns of CoLos upon escapes, and (2) to examine whether CoLos were active during swimming. The latter issue was especially important as this has not been addressed in previous studies

in adult goldfish (Fetcho and Faber, 1988; Fetcho, 1990, 1991).

Recordings were obtained from 25 CoLos (1 at 2 dpf, 11 at 3 dpf, 12 at 4 dpf, and 1 at 5 dpf). Representative examples are shown in Figures 6B and C (3-dpf larva) and Figures 6D-G (4-dpf larva). Upon electrical stimulation near the contralateral ear (asterisks in each panel), VR activities with short latencies from the stimuli were often elicited (marked by "escape" in each panel). These activities likely corresponded to the initial bend associated with escapes. In the early phase of these initial VR activities, CoLos often showed successive spikes (marked by "spikes" in each panel). The first spike in the CoLos always preceded the VR activity (easily seen in the magnified view of Figures 6E and F). This is consistent with the idea that CoLos, whose activities were driven via electrical synapses from the M-axon, fired earlier than motoneurons during escapes (the sites of VR recordings were always rostral to those of CoLo recordings, and therefore, the preceding firing of CoLos was not due to rostro-caudal shift of motor activity). Nineteen out of 25 CoLos fired during at least one stimulation trial. There were age-dependent changes in the number of CoLo spikes per escape. Younger animals tended to show more spikes (an average of 2.79 ± 1.15 for 11 cells at 3 dpf vs. an average of 1.52 ± 0.60 for 8 cells at 4 dpf).

Next, activities of CoLos during swimming were examined. The escape behaviors were usually followed by rhythmic VR activities that corresponded to swimming. CoLo spikes were not observed during this swimming phase (Figs. 6B-D). For each CoLo neuron, at least 5 swimming episodes were elicited with electrical stimulations, but I did not observe any CoLo spikes except for those corresponding to the initial bend of escapes. This was true not only for swimming elicited by electrical

stimulations but also for spontaneous swimming (Fig. 6G) and for light-flash-elicited swimming (data not shown). Thus, I concluded that CoLos were not active during swimming. On the contrary, CoLos received inhibition during swimming. This inhibition was apparent when recordings were made in depolarized conditions with constant positive current injections (dots in Figs. 6C, F and G; chloride reversal potential, -70 mV).

Behavioral experiments: the role of CoLos upon bilateral activation of the M-cells

Based on my dye-coupling evidence, I was confident that the entire population of CoLo neurons was visualized in the Tol-056 fish. This enabled me to examine the behavioral roles of these cells by specifically ablating them by laser. CoLos were expected to play roles in escapes triggered by Mauthner spikes. Therefore, I focused my analyses on sound/vibration-elicited escapes (Fig. 8A), as M-cells have been shown to play a major role in escapes evoked by acoustic-vestibular stimulations in larval zebrafish (Burgess and Granato, 2007; Kohashi and Oda, 2008).

M-cells indeed played a critical role in initiating fast escapes in my experimental system. In response to sound/vibration stimulus, larvae (5.3-5.8 dpf) showed fast escapes (latency < 15 msec; Fig. 8C) in more than 80% of trials. When both of the M-cells were laser-ablated (2 larvae; Fig. 7C), fast escapes (latency < 15 msec) were completely abolished; more than 10 trials were carried out for each larva. When one of the M-cells was ablated (3 larvae; Fig. 7B), larvae performed fast escapes only to the contralateral side of the intact M-cell; more than 8 escapes were examined for each

larva. These results show the critical roles of M-cells in the initiation of fast escapes. It is noteworthy that the directions of the escapes were found to be mostly random (Fig. 8B). This suggests that the stimuli in my experimental system had little laterality in larval zebrafish.

I first investigated the effects of bilateral ablation of CoLos located caudal to the 7th segment (an image of a CoLo-ablated larva is shown in Fig. 7D and E). Dramatic impairments in behavior were often observed (Fig. 8D). The abnormal escape behavior was characterized by straightening of the caudal part of the body, whereas the rostral part of the body turned normally. As a result, a sharp kink was apparent (arrowhead in Fig. 8D). In the straight part, which roughly corresponded to the CoLo-ablated region, bilateral activation of trunk musculature appeared to occur, as inferred by the shortening of the body (Fig. 8F). Such abnormal escapes were observed in around 30% of trials, although occurrence frequency varied from animal to animal (Table 1). In trials in which animals did not show impaired escapes, the escape behaviors were indistinguishable from those of controls (data not shown). This precludes the possibility that the severe impaired-escape phenotypes observed were due to collateral damage related to the laser ablation.

I quantitatively analyzed the behaviors by examining the curvature of the body. I compared the curvature of the body at 6 msec because the phenotype was most evident at this time point (Fig. 8G1). The result is summarized in Figure 8G2. Control fish showed smooth curvature of the body at the caudal two-thirds of body (blue trace). By contrast, after bilateral ablation of CoLos, a sharp peak appeared at the rostral end of the body (at 0.3 body length; red trace). In more caudal regions (0.5-0.8), the curvature

value is close to 0, representing straightening of the body. Standard deviations in this straight region are small, indicating the consistency of the phenotype. The curvature of normal escapes in the CoLo-ablated larvae (green traces) is similar to those seen in controls.

When CoLos caudal to the 11th segment were bilaterally ablated, the kinked region shifted caudally (data not shown). Thus, the straightening of the body in the abnormal escapes was due to the absence of CoLos in the corresponding region.

On what occasions did the larvae show impaired escapes? Given that M-cells are responsible for initiating fast escapes in the system, bilateral contraction observed in the CoLo-ablated region suggests that M-cells fired bilaterally in the impaired escapes. The normal escapes in the CoLo-intact region (rostral part of the body) suggest that CoLo-mediated inhibitions made motor activity unilateral in the corresponding region even in such occasions: if CoLos were intact along the entire length of the body, normal escapes would occur. This notion of unilateral motor output upon bilateral activation of the M-cells is in accord with the results of previous studies on the forced co-activation of the M-axons in adult goldfish (Yasargil and Diamond, 1968). Upon electrical activation of the 2 M-axons in the spinal cord, the output by the trailing M-spike was completely suppressed if the time difference of the 2 spikes was greater than a minimal discrimination time (Yasargil and Diamond, 1968; Diamond, 1971). Taking this into account, my results suggest the following. First, the sound/vibration stimuli employed in the present study often elicited bilateral M-cell activation. Second, normal larvae perform escapes even in such occasions by taking advantage of the spike-timing discrimination circuits in the spinal cord. Third, CoLos play a pivotal role in the circuits

(Fig. 8H): in the absence of CoLos, bilateral muscular contractions occur (Fig. 8I).

To obtain evidence supporting this notion, I performed unilateral ablations of CoLos (caudal to the 7th segment). As expected, abnormal escapes were only observed in the direction of the ablated CoLos (frequency, 36%; Table 1). In these abnormal escapes, I occasionally observed "S-shaped" escapes (Fig. 8E). The caudal part of the body curved in the direction opposite the main direction of the escape. This phenotype is explained by the idea that the excitatory effects of the leading M-spike were overridden by those of the trailing M-spike in the case of unilateral presence of CoLos (Fig. 8J; see the legend for a more detailed explanation). In addition to the S-shaped phenotypes, I observed phenotypes that were similar to the ones obtained in the bilateral ablations (straightening of the caudal region; data not shown). In these cases, the differences in timing of the two M-spikes were likely to be slightly larger. This would lead to the late arrival of the CoLo-mediated inhibition, and thereby, the excitatory effects of the leading M-spike were not overridden, resulting in bilateral contraction.

In other larvae, one of the M-cells was ablated in addition to the bilateral elimination of CoLos. In this condition, bilateral M-cell firing should not occur, and thus, I expected that no stiffened phenotype would appear. I performed experiments in 6 larvae. At least 5 escapes were examined in each larva, and thus, more than 30 escapes were examined in total. In these larvae, abnormal escapes were never observed. The larvae performed normal escapes to the opposite side of the intact M-cell (Fig. 8G2). Collectively, all the results thus far described are consistent with the idea that (1) M-cell co-activations often occurred in my experiments, and that (2) CoLos play a pivotal role in allowing animals to perform escapes upon bilateral activation of the M-cells.

Calcium imaging of M-cells

To further obtain parallel evidence that both M-cells were co-activated by the sound/vibration stimulus, I performed calcium imaging (O'Malley et al., 1996; Takahashi et al., 2002; Kohashi and Oda, 2008). The M-cells were retrogradely labeled with a Ca^{2+} indicator, Calcium Green dextran, and imaged with confocal microscopy. The sound/vibration stimuli were delivered to the animals using the same apparatus described above. Evoked fluorescence response ($\Delta F/F$) in the M-cells was compared to that elicited by antidromic (AD) stimulus applied to the spinal cord at the end of experiments (Kohashi and Oda, 2008).

A representative example of Ca^{2+} imaging is shown in Figure 9. Figures 9A and B show the results of the AD stimulations. Fluorescence responses in each M-cell were evoked in an all-or-nothing manner with steady amplitudes. Figures 9C and E show two examples of Ca^{2+} imaging in the sound/vibration stimulation trials. In the trial shown in Figure 9C, both of the M-cells are likely to have fired, as the normalized $\Delta F/F$ (normalized with the $\Delta F/F$ value of the AD spikes) in each cell was close to 100% (black traces in Fig. 9D). In the trial shown in Figure 9E, only the left M-cell is likely to have fired, since the normalized $\Delta F/Fs$ in the left and right M-cells were close to 100% and 0%, respectively (black traces in Fig. 9F). I defined normalized $\Delta F/F$ greater than 70% as a sign of a spike of the M-cell (Kohashi and Oda, 2008). Figure 9D shows traces of all the trials in which both of the M-cells in the larva were considered to fire (black and gray traces). Figure 9F shows traces of all the trials in which only the left M-cell was considered to fire (black and gray traces). The red trace in each panel shows the average of the traces shown (average of black and gray traces). The vast majority of the

traces reasonably represent co-activation (Figure 9D) and single activation (Figure 9F). I also performed line-scan experiments to obtain results with better time resolution. In trials in which M-cell co-activation is likely to have occurred, no discernible difference in the timing of the activations of the two cells was present, although the movement artifact prevented an examination of fluorescence response during a critical time period (~50 msec after the stimulus) (Fig. 10). Ca^{2+} imaging was performed in 5 larvae in total (3 for the frame scan and 2 for the line scan), and co-activations of the M-cells were observed at least once in all the larvae. In total, 23 out of 42 trials (55%) were considered to be co-activations (only those trials in which at least one of the M-cells was judged to have fired were included in the total number). These results support the conclusion that the two M-cells in larval zebrafish were often co-activated upon the sound/vibration stimulations employed in this study.

Rare occurrence of M-cell co-activations within a minimal discrimination time

It has been shown in a previous study that electrically activating both M-axons within a minimal discrimination time results in no motor activity (Yasargil and Diamond, 1968). This may be explained by the idea that CoLo-mediated crossed inhibitions shunt all the excitations (Fig. 11B). Because M-cell co-activation often occurred in my experiments, one might wonder whether co-activations within a minimal discrimination time might have occurred. I assessed this possibility by unilateral ablation of CoLos caudal to the 7th segment, the experiment described in the previous section. The predicted behavior was that in which curvature of the body occurs only in the caudal region where CoLos

are unilaterally present (Fig. 11C). In my experiments, I did observe one such

phenotype (Fig. 11A). However, occurrence of this phenotype was rare, compared to

that of the stiffened (or S-shaped) phenotypes (in total, 12 such phenotypes in fish

#8-14; Table 1). This suggests that the vast majority of the M-cell co-activations were

those in which the differences in timing of the two spikes were beyond a minimal

discrimination time.

DISCUSSION

I have identified a class of commissural inhibitory neurons, CoLos, in larval zebrafish. I have shown that (1) these neurons are present at one cell per hemi-segment; (2) they are electrotonically excited by the M-axon; (3) they provide inhibition to contralateral primary motoneurons; (4) they are active only during the early phase of escapes; and (5) they play an important role in escape behavior upon sound/vibration stimuli. I have provided evidence which strongly suggests that CoLos play a particularly important role upon bilateral activation of the two M-cells: CoLo-mediated spinal inhibitory circuits enable animals to perform escapes in these occasions by suppressing the excitatory effects of one of the M-spikes. This study illustrates a clear case of the behavioral role of a class of interneuron in the vertebrate spinal cord.

Distribution, morphology, and synaptic targets of CoLos

CoLo-corresponding neurons have been identified in adult goldfish and tench (Fetcho and Faber, 1988; Yasargil and Sandri, 1990). However, no information has been reported on the timing of their development. I have shown that CoLos are present even in the embryonic stage, and that they are present at approximately one cell per hemi-segment. This is in accord with the electron micrograph study in adult tench (Yasargil and Sandri, 1990). Thus, once CoLos' segmental distribution is generated in the early stages, the pattern is likely to be maintained throughout life. To my knowledge, CoLo distribution represents the strongest case of segmental pattern of interneuron

distribution in vertebrates. From a developmental point of view, how this segmental distribution is established during development is an interesting issue for future studies.

The critical feature of CoLos is that they receive electrotonic inputs from the M-axon. It is not clear whether the connection was purely electrotonic: there might be additional chemical components, which could have been diminished by cholinergic neurotransmission blockers used for immobilizing animals (M-cells are thought to be cholinergic; Day et al., 1983). Importantly, however, electrotonic inputs alone were sufficient to drive spikes in CoLos. Neuronal type connexin was found to be densely present at the Mauthner-CoLo synapses, suggesting a large electrotonic conductance. This probably contributed to the reliable induction of CoLo spikes upon M-spikes.

The configuration of the Mauthner-CoLo circuits is ideal for producing very fast crossed inhibition upon receiving an M-spike. These include (1) fast electrical transmission; (2) a robust CoLo axon (indicative of fast conduction); (3) a descending main axon (in the same direction that the M-spike travels); and (4) short axons (though robust, CoLo-axon conduction velocity is likely to be slower than that of the giant M-axon). With chains of short inhibitory neurons, the opposite side can receive inhibition with a minimal delay. Regarding the postsynaptic targets of CoLos, direct evidence is only available for primary motoneurons. However, all the known targets of the M-axon, including CoLos, have been shown to receive very fast inhibition upon a contralateral M-spike, strongly suggesting that CoLos inhibit all of these (Fetcho, 1990). My own and previous anatomical studies also support this view (Yasargil and Sandri, 1990; Fetcho, 1990).

Escape-specific activity of CoLos

To what extent the activity of spinal interneurons is shared by different motor activities is an important issue. Fetcho (1991) pointed out a similarity between Mauthner-mediated escape circuits in fish and swimming circuits in tadpoles and lamprey, raising the possibility that some of the circuit components might be shared between these two behaviors. At least for CoLos, however, this is not the case: CoLos were never active during swimming. The same conclusion was recently reported by (Liao and Fetcho, 2008), where the authors further showed that CoLos were not active during struggling, a very strong but slower movement. A likely reason why the spinal cord contains this specialized class of neurons is that the speeds required for escapes and swimming/struggling differ greatly; inhibition mediated by the commissural interneurons without CoLos would not be fast enough for escapes.

The present study has focused on the role of CoLos in escapes that occur from rest (see the following section). However, fast escapes are known to occur when fish are swimming by immediately shutting down the ongoing activity (Jayne and Lauder, 1993; Svoboda and Fetcho, 1996). Eaton et al. (1995) suggested that one of the primary roles of the large M-axons are to turn off competing contralateral activity. I expect that fast crossed inhibitions mediated by CoLos play an important role in this process by immediately shunting motoneuron activities. Future studies must address this issue.

Escape behaviors in fish are a form of startle response. Startle responses occur in a wide variety of species including mammals. Like Mauthner-mediated escape behaviors in fish, one characteristic feature of the acoustic startle response in mammals is the immediate arrest of ongoing activity (Eaton, 1984). This suggests the involvement

of short-latency inhibition. With analogy to CoLos, it would be interesting to ask whether the mammalian spinal cord contains inhibitory interneurons dedicated to startle responses.

The role of CoLos in escapes upon bilateral activation of the M-cells

CoLo-ablated larvae often showed impaired escapes upon sound/vibration stimuli. Thus, CoLos, with a presence of just one cell per hemi-segment, play very important roles in escape behavior. I have obtained several lines of evidence which strongly support the notion that both of the M-cells were activated in these impaired escapes. This in turn suggests that, in normal conditions, larvae are able to perform escapes upon M-cell co-activation by taking advantage of CoLo-mediated inhibitory circuits in the spinal cord. My calcium imaging data also suggest that co-activations of the M-cells did occur upon the sound/vibration stimuli employed in my study.

The present study uncovers the behavioral importance of the spike-timing discrimination circuit that was first described by Yasargil and Diamond (1968). They showed that the spinal circuits could discriminate slight differences in timing of the M-spikes; when both of the M-axons were artificially activated, the excitatory effect of the trailing spike was completely suppressed if the intervals of the spikes were greater than the minimal discrimination time (around 0.15-0.20 msec in adult goldfish). The importance of this, however, has not been fully emphasized, as subsequent evidence showed that in the vast majority of escapes only one of the M-cells fired (Zottoli, 1977; Eaton et al., 1981). My results strongly suggest that co-activation of the two M-cells do occur in escapes elicited by sound/vibration stimuli having little laterality, and that

CoLos lie at the core of this spike-timing discrimination circuit. As discussed above, CoLos' configuration is ideal for shunting all the excitatory effects of the trailing M-spike. This circuit is likely to be behaviorally important for fish in their natural lives. Predator attacks do not always have laterality (e.g., attacks from above). Upon an attack, an animal may need to perform an escape to either direction. The CoLo-mediated discrimination circuit enables animals to do so.

M-cell co-activation is not likely to be specific to larval fish. Firing of the M-cell on the side of the escape was reported in adult goldfish (Zottoli, 1977; Eaton et al., 1988), although the occurrence frequencies were much lower (1/39 and 1/16, respectively). In such "incorrect" firings, it is likely that the other M-cell fired earlier. In the present study, larval zebrafish showed a higher frequency of M-cell co-activation (around 30% in the behavioral experiments). Differences in laterality of the stimuli used in the different experiments could explain the difference in frequency. In addition, adult fish may have better ability to detect slight laterality by utilizing multiple layers of inhibitory circuits in the hindbrain (Korn and Faber, 2005). It is important to note, however, that many of the inhibitory circuits, including reciprocal inhibitions of the two M-cells, are already functional in 5-dpf zebrafish larvae (Takahashi et al., 2002). Therefore, the frequent co-activation of the two M-cells in the present study could not be attributed to the absence of the reciprocal inhibition circuit of the two M-cells.

Takahashi et al. (2002) suggested that the reciprocal inhibitions arrive within 2 msec. Thus, in my experiments, bilateral activation of the M-cells perhaps occurred within this narrow time window. The phenotype of CoLo-ablated animals also supports this view: bilateral muscular contractions appeared to occur near-simultaneously.

Nonetheless, my results also suggest that M-cell co-activation within a minimal discrimination time rarely occurs, meaning that the two spikes are slightly de-synchronized. The M-cell is known to receive a large amount of spontaneous inhibitory inputs (Hatta and Korn, 1999; Korn and Faber, 2005), which probably help de-synchronize the two M-spikes.

The spinal cord tends to be considered as output machinery that just obeys descending commands. However, the spinal circuits in fish can neglect a trailing M-spike, which, if occurring alone, produces a very powerful output. This means that descending motor commands are filtered in the spinal cord to produce the appropriate behavior. Although the case might be an exceptionally dramatic one, information processing of descending commands at the level of the spinal cord might be more important than generally considered for the proper execution of behaviors in vertebrates.

FIGURES and TABLE
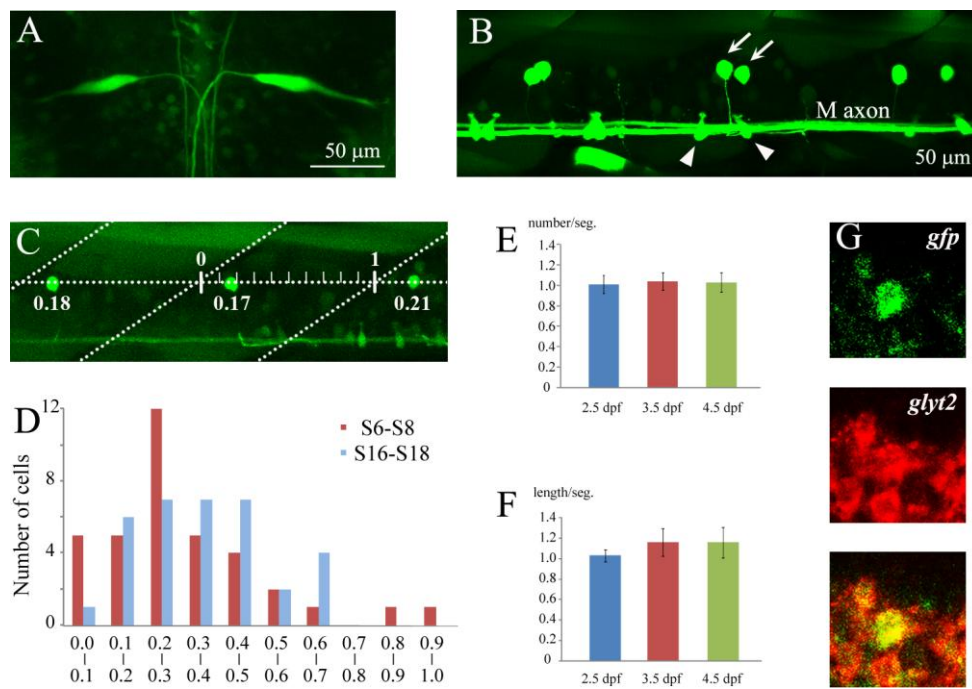
Figure 1. GFP expression in the Mauthner cells and CoLo neurons in the Tol-056 enhancer trap line.

A, Dorsal view of a 4-dpf larva. Rostral is to the top (the same for all subsequent figures of dorsal views). Stacked image of confocal optical sections. GFP expression is present in a pair of Mauthner cells in the hindbrain. **B**, Lateral view of the spinal cord of a 4-dpf larva. Dorsal is to the top, and rostral to the left (the same for all subsequent figures of lateral views). Stacked image of confocal optical sections. GFP expression is present in the Mauthner (M) axon, Kolmer-Agduhr (KA) neurons (arrowheads), and CoLo neurons (arrows). **C**, Plots of the number of CoLo neurons (per hemi-segment) versus developmental age. Number of CoLos located between the 8th and 17th segments (10 segments) was counted in 10 fish (100 segments in total) at each age. Throughout all ages, the number of CoLos was approximately one per hemi-segment. **D**, Lateral view of the spinal cord of a 3.5-dpf larva. Dashed lines demarcate segment boundaries. Hash marks indicate basis for numerical position measurements (labeled under the CoLo neurons). **E**, Plot of the number of CoLo neurons versus their position. Three segments of the rostral region (segments 6-8; red bar) and three of the caudal region (segments 16-18; blue bar) were examined from 10 fish at 3.5 dpf (30 segments were examined for each region). Total CoLo cell numbers for each region are 36 (S6-S8) and 34 (S16-18). **F**, Double in situ hybridization of *gfp* and *glyt2* in a 3-dpf larva. The *gfp*-positive CoLo neuron was also positive for *glyt2*.
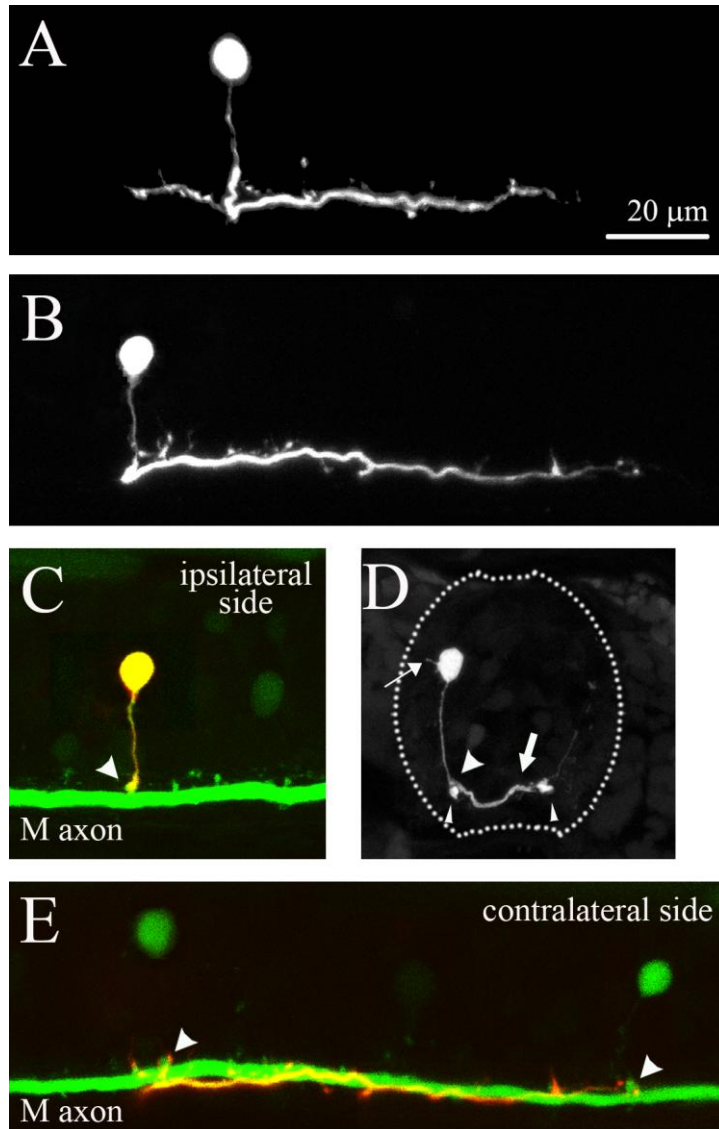
Figure 2. Morphology of CoLo neurons.

Rhodamine-dextran was loaded to individual CoLo neurons by electroporation. **A**, A confocal stacked image of a CoLo neuron at 3 dpf. **B**, A confocal stacked image of a CoLo neuron at 4 dpf. **C**, The same sample as the one shown in **B.** Only the optical sections on the ipsilateral side are stacked. Green indicates GFP signal, whereas red indicates rhodamine signal. Because the rhodamine-labeled CoLo neuron also had GFP, the CoLo neuron is indicated by a yellow signal. The arrowhead indicates the contact sites between the M-axon and the CoLo axon. The contact sites are evident as lumps of GFP signal. The lumps are more clearly visible in **E. D**, A cross-section. The thin arrow shows a dendritic process. The slim arrowheads show the M-axons. The thick arrow shows a CoLo axon crossing the spinal cord. The fat arrowhead indicates the contact site between the CoLo axon and M-axon. **E**, The same sample as the one shown in **B.** Only the optical sections on the contralateral side are stacked. The two green cells are CoLo neurons on the contralateral side (different from the rhodamine-labeled CoLo neuron). The arrowheads indicate the contact sites between the M-axon and the axons of the contralateral CoLos. The contact sites are evident as lumps of GFP signal. Processes from the rhodamine-labeled CoLo axon appear to terminate near the contact sites.

F, Plots of the length of the CoLo axon. For each rhodamine-labeled CoLo neuron, the rostral and caudal ends of its axon on the contralateral side were determined. The length between the rostral and caudal ends was measured, and divided by the average length of a segment at each developmental age. Numbers of CoLo neurons examined for each age are: 4 at 2.5 dpf, 8 at 3.5 dpf, and 5 at 4.5 dpf.
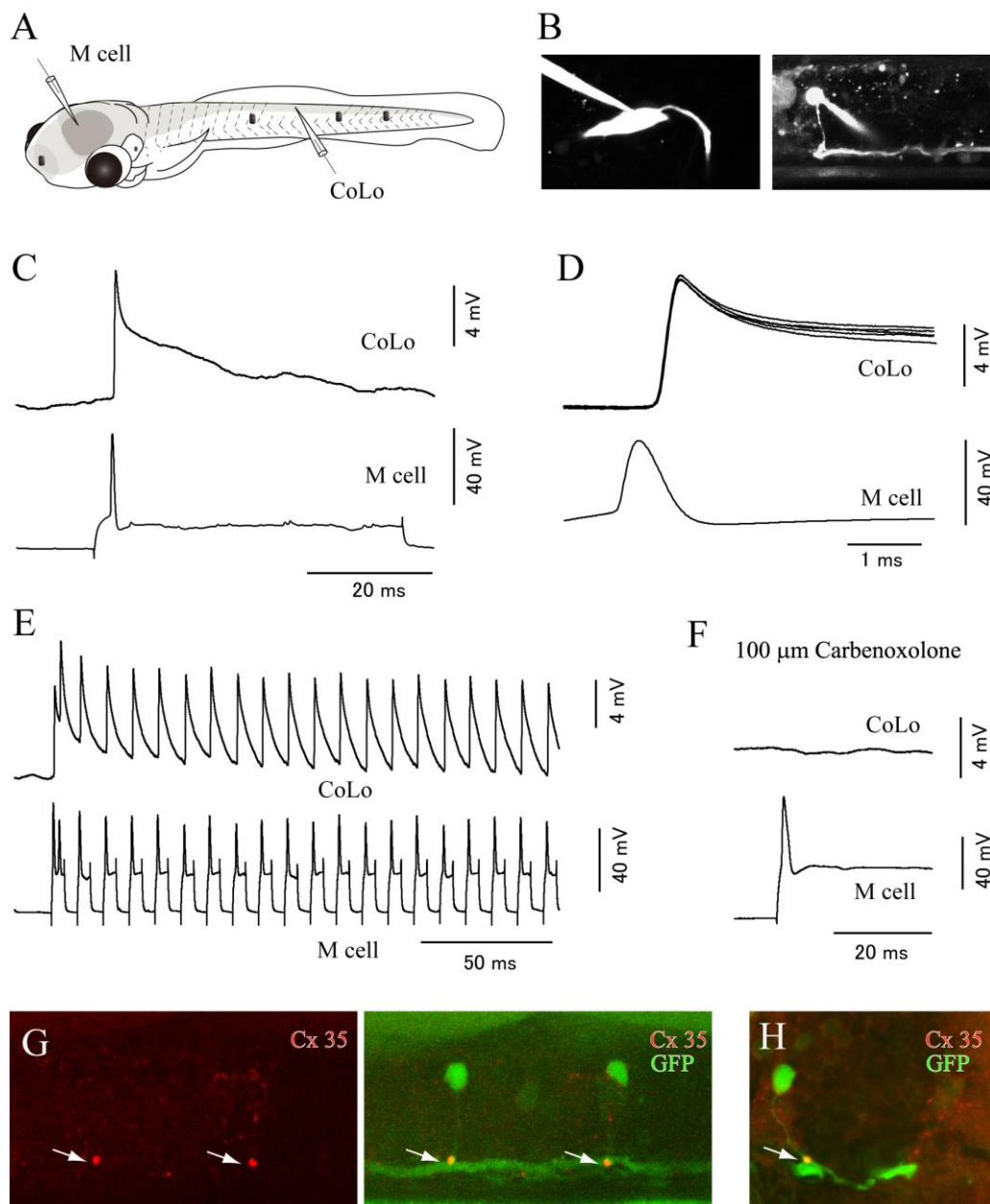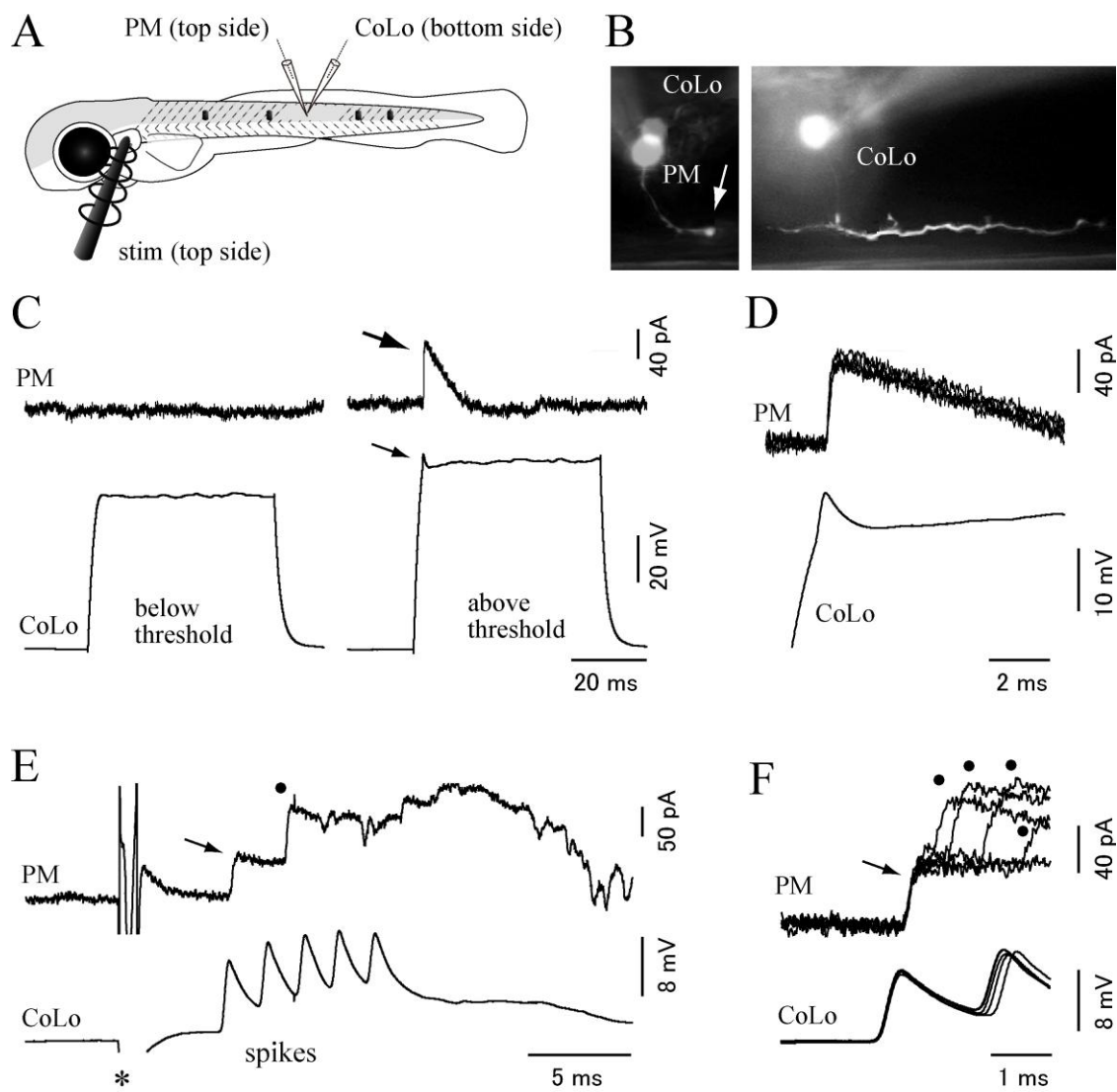
Figure 3. The Mauthner cell makes electrical synapses onto CoLo neurons.

A, A schematic illustration of the paired patch recordings between a Mauthner (M) cell and a CoLo neuron. The black dots represent tungsten holding pins. **B,** Images of the M cell (left) and the CoLo neuron (right) after the electrophysiological recordings shown in **C-F**. Four-dpf larva. **C,** The current-evoked spike of the M-cell led to a fast and sharp depolarizing response (approximately 10 mV in amplitude) in the CoLo neuron. This sharp depolarizing response represents a spike in the CoLo neuron (see Fig. 5 and text). **D**, Five superimposed traces of CoLo spikes evoked by M-cell spikes. The traces show short, constant latency spikes. Only one spike in the M-cell is shown for simplicity. Traces of voltage responses in the CoLo neuron are aligned with the peak of the spikes in the M-cell. **E**, Responses of the CoLo neuron upon 100-Hz spikes of the M-cell. CoLo spikes perfectly followed M-spikes with the same amplitude in each spike. **F,** Response of the CoLo neuron was eliminated after treatment with 100 μm of Corbenoxolone (a gap junction blocker) for 15 min. **G**, Lateral view of immunostaining with Cx35 (Connexin35). A stacked image of confocal optical sections. The left panel shows staining of Cx35, whereas the right panel shows a merged image of Cx35 and GFP. The intense Cx35 signals (arrows) are observed at the contact sites between CoLo axons and the M-axon. **H,** A cross-section. The arrow shows an intense signal of Cx35.
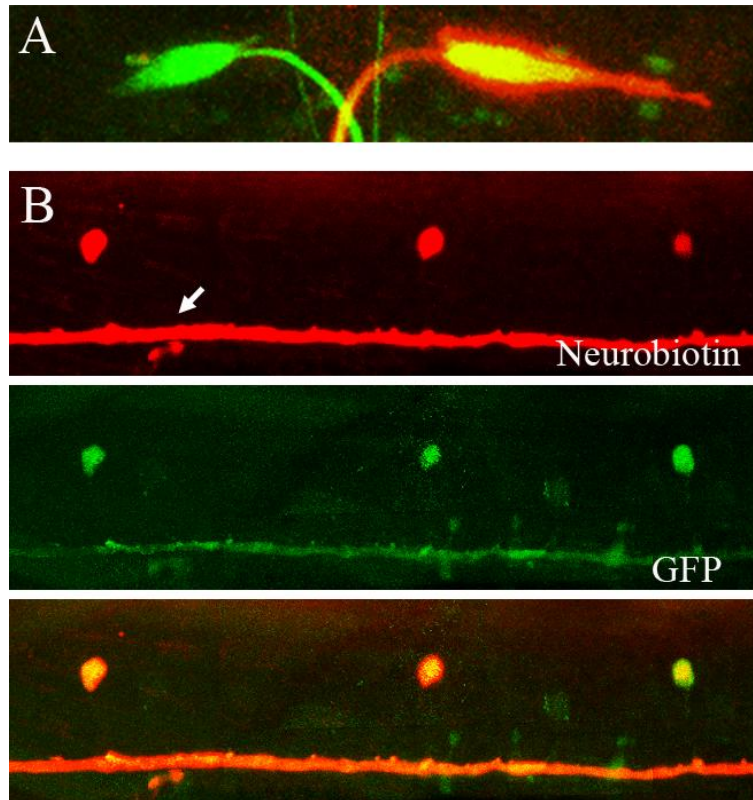
**Figure 4. Dye-coupling between the Mauthner cell and CoLo neurons.**

Neurobiotin was loaded into one of the M-cells in a 3-dpf larva, and the sample was processed for neurobiotin staining. **A,** In the hindbrain, one of the M-cells along with its axon shows neurobiotin staining (red signal). **B,** In the spinal cord, CoLo neurons as well as the M-axon (arrow) show neurobiotin staining, indicating that the CoLo cells are connected to the Mauthner axon via gap junctions.

A PM (top side) CoLo (bottom side)

stim (top side)

B CoLo PM CoLo

C PM 40 pA 20 mV below threshold above threshold 20 ms

CoLo

D PM 40 pA 10 mV 2 ms CoLo

E PM 50 pA 8 mV CoLo spikes * 5 ms

F PM 40 pA 8 mV CoLo 1 ms

Figure 5. Paired recording between the CoLo neuron and the primary motoneuron.

A, A schematic illustrates the paired recording shown in **B-F**. The recording was made using a 3-dpf larva. A stimulation electrode was placed near the ear on the top side. One patch electrode was placed targeting the primary motoneuron (PM) on the top side, while the other patch electrode was placed targeting the CoLo neuron on the bottom side. The black dots represent tungsten holding pins. **B,** The pictures show images of the recorded cells. Montages were made to show the morphology of each cell. The left panel shows the morphology of a primary motoneuron. The arrow shows its torn axon at the edge of the spinal cord. The image of a CoLo soma located on the opposite side of the spinal cord is superimposed for the comparison of relative locations of the two cells. The right panel shows the morphology of the CoLo neuron. **C,** In this experiment, and the experiments shown in **D-F**, the CoLo neuron was recorded in a current clamp mode, whereas the primary motoneuron was recorded in a voltage clamp mode with the holding potential at -50 mV. The chloride reversal potential calculated with the experimental condition is -70 mV. The left panel shows that there was no response in the primary motoneuron when the depolarizing pulse in the CoLo was below threshold, whereas the right panel shows that, upon a current pulse above the threshold, an evoked CoLo-spike (thin arrow) leads to an IPSC in the primary motoneuron (thick arrow). **D,** Five superimposed traces of IPSCs in the primary motoneuron. The traces show short, constant latency IPSCs. Only one spike in the CoLo neuron is shown for simplicity. **E,** Responses of the CoLo neuron and the primary motoneuron upon an escape trial. An

electrical stimulation was applied at the time point marked by the asterisk. With a short latency from the stimulus, the CoLo neuron expressed several successive spikes (labeled as "spikes"). These spikes likely correspond to the activity associated with an escape (see Fig. 6). The primary motoneuron received IPSCs during the escape. The timing of the earliest IPSC (arrow) coincides with the first CoLo spike. The timing of the second IPSC (dot) does not coincide with any of the CoLo spikes. **F,** Five superimposed traces of IPSCs in the primary motoneuron, and spikes in the CoLo neuron. In all traces, the timings of the earliest IPSCs (arrow) perfectly coincide with those of the first CoLo spikes. Subsequently, the primary motoneuron received IPSCs at various timings (dots) that are not related to CoLo spikes.
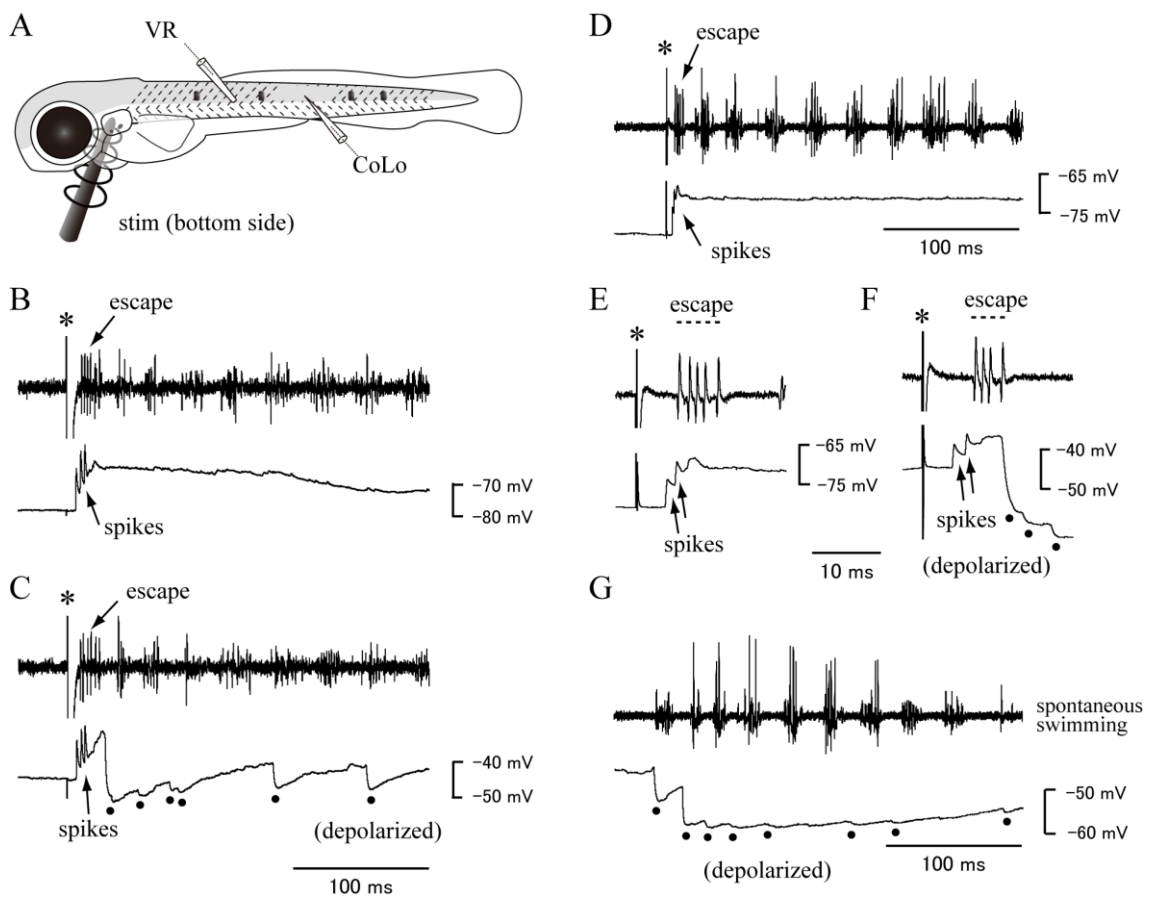
Figure 6. Activity of the CoLo neurons during fictive locomotion.

A, A schematic illustrates the recordings shown in **B-G**. In **B-G**, the top of each panel shows the VR recording, whereas the bottom shows the whole-cell recording of the CoLo neuron. **B** and **C,** Recordings in a 3-dpf larva. Electrical stimulations were applied at the time points marked by asterisks (the same for **D-F**). Upon stimulations, VR activity occurred with short latencies from the stimuli (labeled as "escape"). This VR activity likely corresponds to the initial escape bend. During the escapes, the CoLo neuron expressed successive spikes (the neuron fired 3 times in **B** and **C**). Following the escapes, rhythmic VR activity corresponding to swimming occurred. The cell did not fire during the swimming phase. Instead, the cell received inhibition during swimming. This inhibition is clearly seen in **C** (dots), where the recording was performed in a depolarized condition with a constant positive current injection. **D-G**, Recordings in a 4-dpf larva. **D** and **E**, Upon stimulation, an escape occurred (labeled as "escape"). **E** shows a close-up view of **D** during the escape. The CoLo neuron fired twice in this trial. The cell did not fire during the swimming phase. **F,** An escape trial was made during the recording of a depolarized condition. Close-up view. After the escape, the cell received inhibition (dots). **G**, VR activity during spontaneous swimming. The recording was performed in a depolarized condition. The cell received inhibition during swimming (dots).
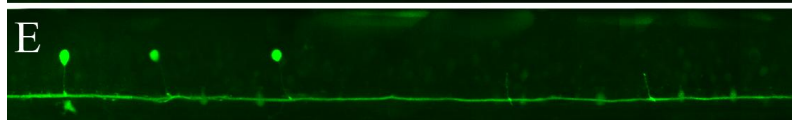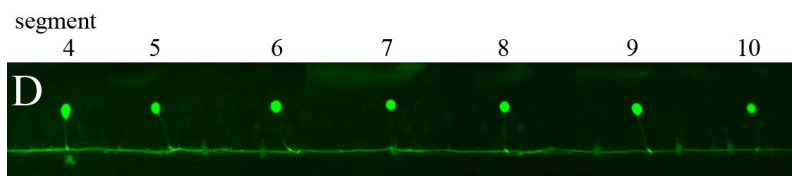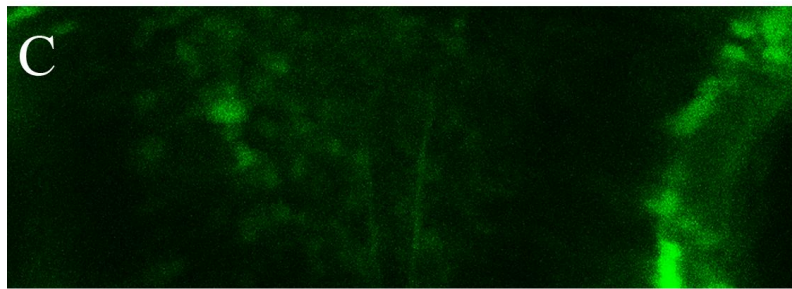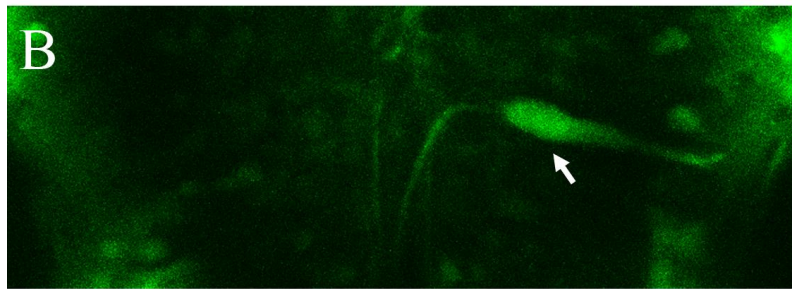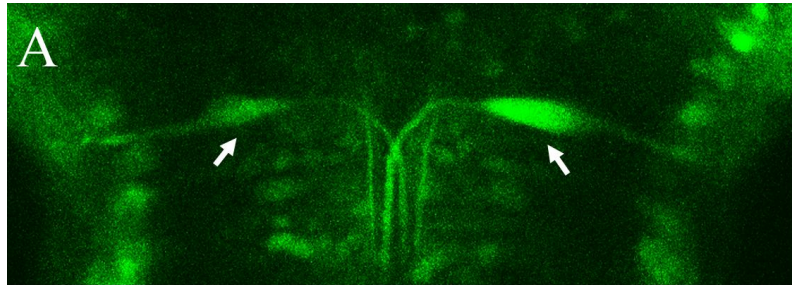
Figure 7. Laser ablation of M-cells and CoLo neurons.

A-C, Dorsal view of the hindbrain at 3.5 dpf. The arrows indicate GFP-labeled M-cells.

A, An image of a control larva. **B**, An image of a larva in which the left M-cell was

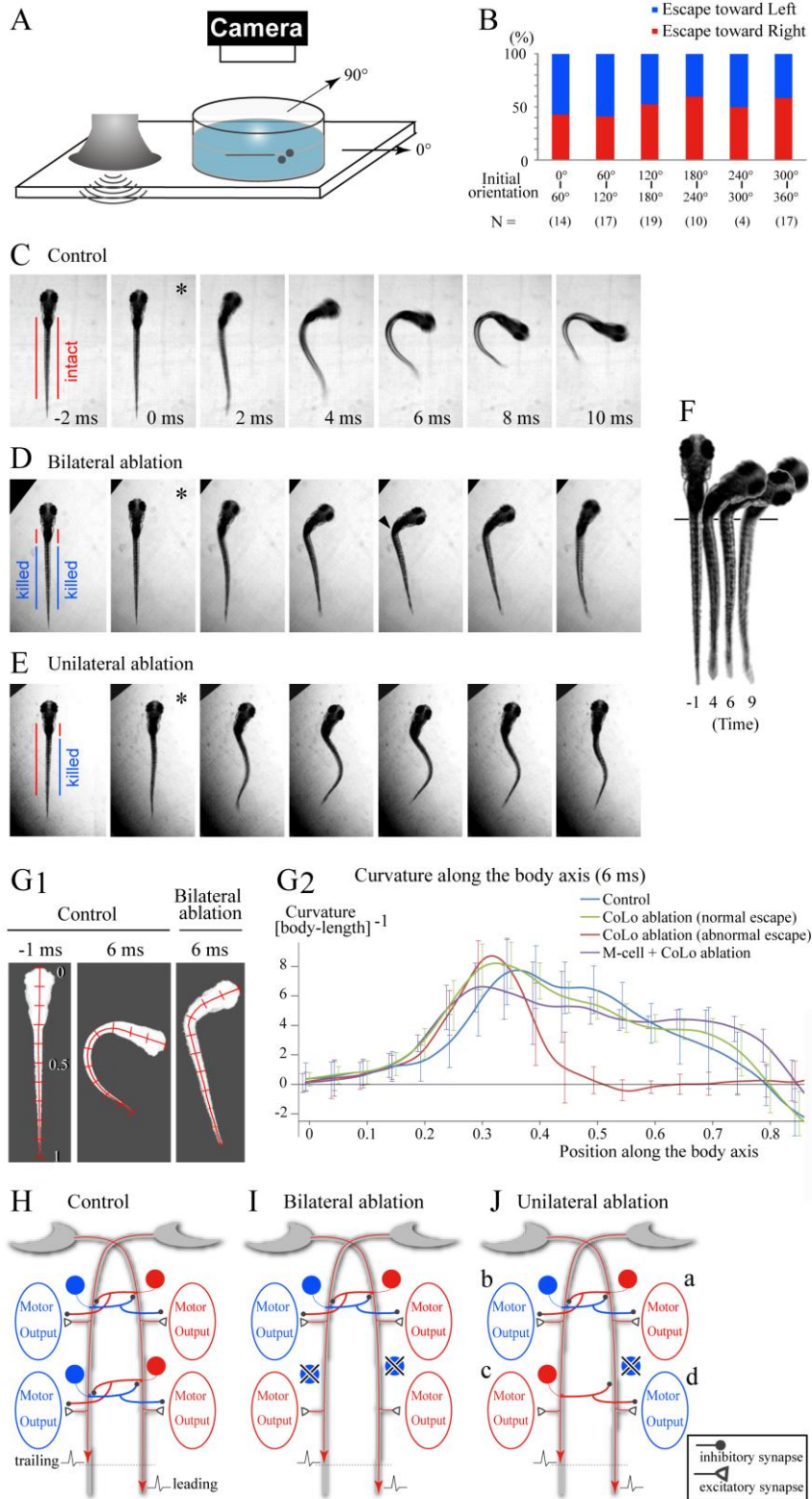ablated by laser. **C**, An image of a larva in which both of the M-cells were ablated by

laser. **D,E,** Laser ablation of CoLo neurons. Laser ablation was carried out against CoLo

neurons located caudal to the 7th segment. Lateral view of the spinal cord at 2.5 dpf.

Only one side of the spinal cord is shown. **D,** An image taken before laser ablation. **E,**

An image of the same larva taken 40 minutes after laser ablation.

A

Camera

90°

0°

B

(%)

- Escape toward Left
- Escape toward Right

100

50

0

Initial orientation	0°↓60°	60°↓120°	120°↓180°	180°↓240°	240°↓300°	300°↓360°
N =	(14)	(17)	(19)	(10)	(4)	(17)

C Control

intact

-2 ms   0 ms   2 ms   4 ms   6 ms   8 ms   10 ms

D Bilateral ablation

killed   killed

E Unilateral ablation

killed

F

-1 4 6 9
(Time)

G1

Control   Bilateral ablation

-1 ms   6 ms   6 ms

0

0.5

1

G2 Curvature along the body axis (6 ms)

Curvature [body-length]$^{-1}$

- Control
- CoLo ablation (normal escape)
- CoLo ablation (abnormal escape)
- M-cell + CoLo ablation

8

6

4

2

0

-2

0   0.1   0.2   0.3   0.4   0.5   0.6   0.7   0.8

Position along the body axis

H Control

Motor Output   Motor Output

Motor Output   Motor Output

trailing   leading

I Bilateral ablation

Motor Output   Motor Output

Motor Output   Motor Output

J Unilateral ablation

b   a

Motor Output   Motor Output

c   d

Motor Output   Motor Output

- inhibitory synapse
- excitatory synapse

Figure 8. Behavioral analyses of the CoLo-ablated larvae.

A, A schematic illustration of the experimental set-up. Sound/vibration generated in the audio speaker propagates to the Petri dish. This elicits an escape in a larva. **B,** Relationships between the initial orientation of the larvae (see the schematics in **A**) and the direction of the escape. "N" stands for the number of the trials. The number of larvae used in this experiment was 16. **C, D** and **E,** Escape responses of a control (**C**) and CoLo-ablated larvae (**D** and **E**). In each panel, a single asterisk marks the initiation of movement. Images were collected at 1,000 frames/sec. Every other frame is shown (2 msec between frames). **C,** An example of an escape behavior in a control larva (a Tol-056 heterozygote). **D,** An example of an abnormal escape behavior in a CoLo-ablated larva (bilateral ablation of CoLos located caudal to the 7th segment). Note that the caudal part of the body is almost straight, while contraction of the rostral part of the body seems normal. This resulted in a sharp kink (arrowhead). **E,** An example of an abnormal escape behavior in a CoLo-ablated larva (ablation of the right-side CoLos located caudal to the 7th segment).. Note that, near-simultaneously, the rostral part of the body curved toward the right, whereas the caudal part of the body curved toward the left. This resulted in a characteristic S-shape of the body. **F,** Images of the bilaterally ablated larva at 4 different time points (the same trial shown in **D**). The onset of movement is defined as time 0. The pigmentation pattern was used to align larvae (the vertical line). Note that the straight part of the body is shortened. **G1,** Midline tracing of larvae. Images were inversed, and the midline was traced. Position along the body axis is indicated by bars at increments of 0.1. Left, a control larva before

movement; Center, a control larva at 6 msec after the onset of movement; Right, a

bilaterally CoLo-ablated larva at the 6-msec time point. **G2**, Quantitative analyses of the

curvature of the body at the 6-msec time point. Curvature of the midline at 0.001

increments of body length was calculated with BohBoh software. The blue trace

represents the mean value of the escapes of control larvae. The green trace represents

the mean value of the normal escapes of bilateral CoLo ablations. The red trace

represents the mean value of the abnormal escapes of bilateral CoLo ablations. The

purple trace represents the mean value of the escapes in those larvae in which unilateral

ablation of the M-cell and bilateral ablation of CoLos were carried out. The numbers of

images examined are: 14 for control; 18 for bilateral ablation with normal escapes; 9 for

bilateral ablation with impaired escapes; 11 for unilateral M-cell ablation and bilateral

CoLo ablation. For every 0.05 increment of position, the standard deviations are

indicated. **H, I**, and **J**, Schematic illustrations for explanation of the motor activities in

control (**H**), bilaterally ablated (**I**), and unilaterally ablated (**J**) larva upon co-activation

of the two M-cells with slight time differences. In each panel, the leading spike runs on

the right M-axon. Circular cells represent CoLo neurons. Red represents an active state,

whereas blue represents an inactive state. **H**, The motor activity on the left side along

the entire body is suppressed by the crossed inhibitions mediated by CoLos, resulting in

a normal escape toward the right. **I**, In the rostral part of the body where CoLos are

present, the motor activity of the left side is suppressed. In the caudal part where CoLos

are absent, both sides become active, resulting in the straightening of the body. **J**, In the

rostral part where CoLos are present, the right side is active (a), whereas the motor

activity of the left side is suppressed by CoLos (b). In the caudal part, where CoLos are

absent on the right side, the activity occurs on the left side (c). Activation of the right

side depends on the balance between the excitatory effects originating from the right

M-spike and the inhibitory effects originating from contralateral CoLos. If the

inhibitions arrive early enough, the excitatory effects are suppressed (d).

A Antidromic stim.

B

C

D

E

F
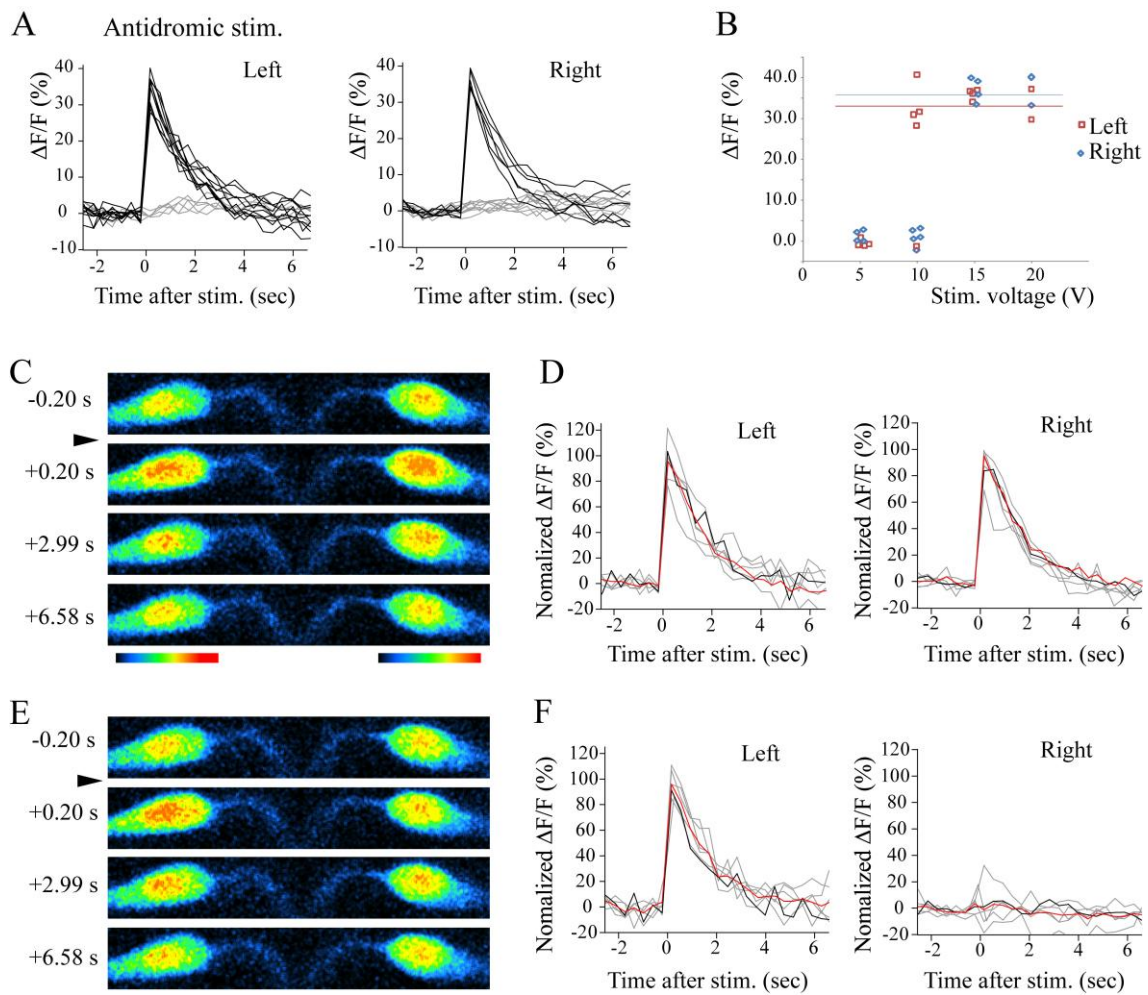
Figure 9. Fluorescence responses of the paired M-cells upon sound/vibration stimuli.

A, Plots of fluorescence responses associated with an antidromic (AD) spike of the M-cells. The responses occurred in an all-or-nothing manner. The black traces represent supra-threshold responses. The gray traces represent sub-threshold responses. **B**, The amplitude of the fluorescence response upon electrical stimulation in the spinal cord is plotted against stimulation intensities. The constant responses to the supra-threshold stimuli are consistent with the generation of a single antidromic spike. The average values of the responses (36.1% for the left M-cell; 33.9% for the right M-cell) were used to normalize the fluorescence responses shown in **D** and **F**. **C**, An example of co-activation of the M-cells upon a sound/vibration stimulus. Pseudocolored images of the fluorescence responses before (-0.2 s) and after (+0.20 s, +2.99 s and +6.58 s) the sound/vibration stimulus. For the purpose of illustration, different look-up tables, shown under the panels, were used to make the images on the left and the right. This is because the labeling intensities of the left and right M-cells were different. The left and right images were combined. **D**, Plots of the fluorescence of the M-cells upon sound/vibration stimuli. Fluorescence responses ($\Delta F/F$) were normalized with the values associated with the AD stimulations. All the trials in which both of the M-cells in the larva were considered to have fired (> 70% of normalized $\Delta F/F$) are shown (black and gray). The black trace corresponds to the trial shown in **C**. The responses of the rest of the trials (n=6) are shown in gray. The red traces represent the averages. **E**, An example of activation of a single M-cell upon a sound/vibration stimulus. The same look-up

tables employed in **C** were used to make the left and right images. **F**, Plots of the

fluorescence of the M-cells upon sound/vibration stimuli. All trials in which only the

left M-cell was considered to have fired are shown (black and gray). The black trace

corresponds to the trial shown in **E**. The responses of the rest of the trials are shown in

gray (n=6). The red traces represent the averages.
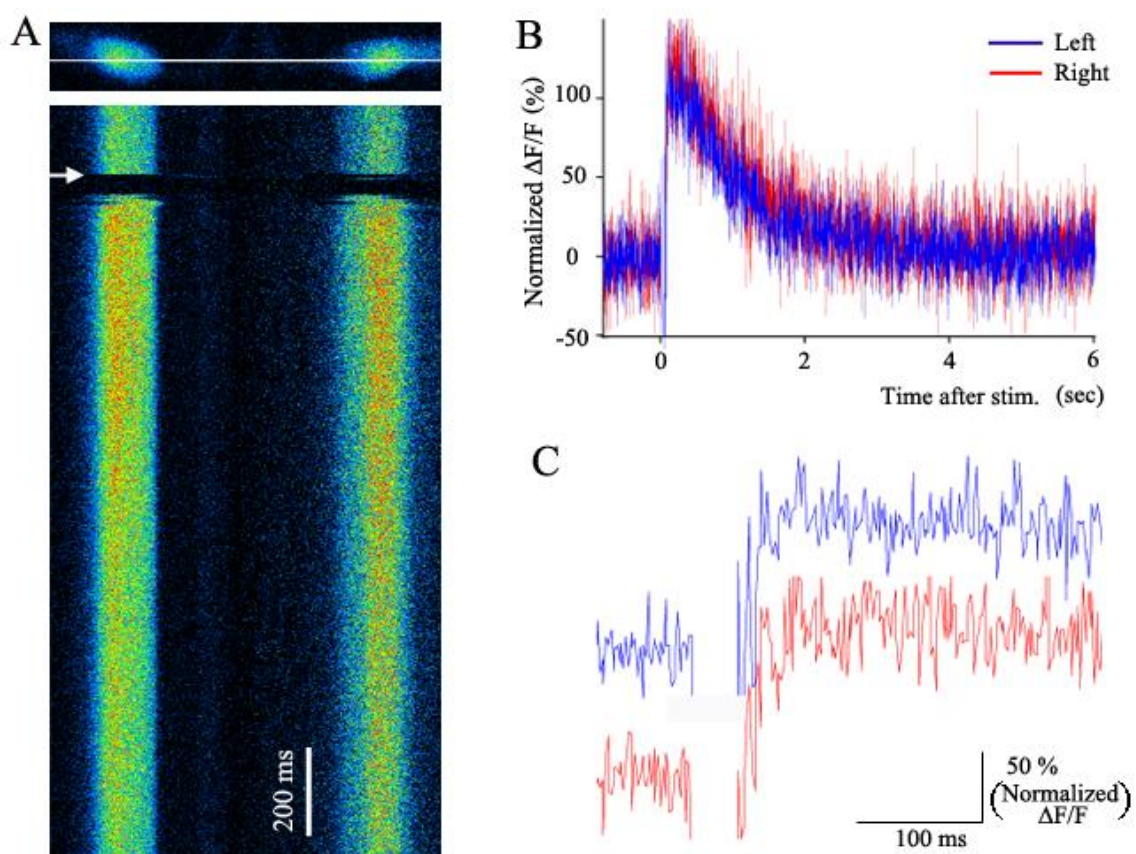
Figure 10. An example of the confocal line-scan experiment in the paired M-cells.

A, The fluorescence of a line (white line in the top panel) that passed through both of the M-cells was monitored repeatedly as shown in the bottom panel. Consecutive lines were acquired at 2 msec intervals and are displayed from top to bottom. For the purpose of illustration, different look-up tables were used to make the images on the left and the right. The left and right images were combined. A sound/vibration stimulus was applied at the time-point indicated by the arrow. Movement of the head associated with the stimulus and the subsequent escape caused the displacement of the cells, resulting in the disappearance of the cell image (~50 msec of blank time in total). Following this blank time, an increase in fluorescence is apparent in both of the cells. **B**, Plots of the fluorescence responses of the two M-cells in the experiment shown in the left. Fluorescence responses (ΔF/F) were normalized with the values associated with the AD stimulations. **C**, a close-up view of **B** during the stimulus and the subsequent escape.

Probable behaviors upon M-cell co-activation within a minimal discrimination time
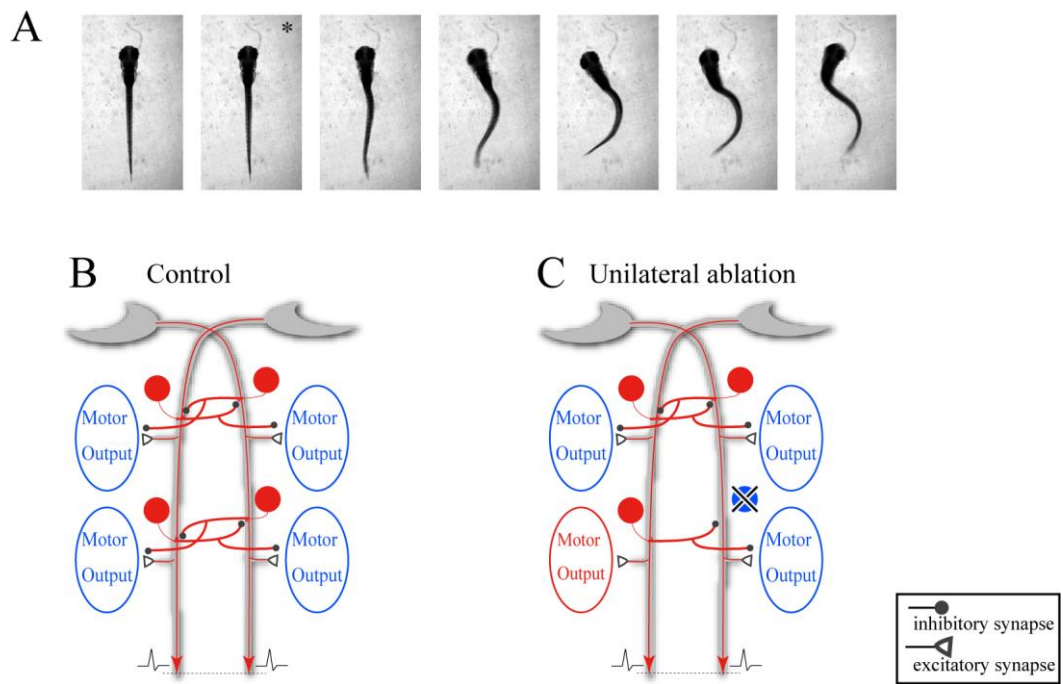
Figure 11. Probable behaviors upon M-cell co-activation within a minimal discrimination time.

A, An example of an abnormal escape behavior in a CoLo-ablated larva (ablation of the right-side CoLos located caudal to the 7th segment). In each panel, a single asterisk marks the initiation of movement. Images were collected at 1,000 frames/sec. Every other frame is shown (2 msec between frames). Note that, only the caudal part of the body curved toward the left. **B,C,** Schematic illustration for explanation of a control larva larva nad ablated larva. Red represents an active state, whereas blue represents an inactive state. **B**, Schematic illustration for explanation of a control larva. Motor activity along both sides of the entire body is suppressed by CoLo-mediated crossed inhibition, resulting in no movement. **C**, Schematic illustration for explanation of a larva in which CoLos on the right side (caudal to the 7th segment) were ablated. In the rostral part where CoLos were present, there was no activity on either side, as in the control. In the caudal part, motor activity on the left side occurred owing to the unilateral absence of CoLos.

	Number of total escapes	Number of impaired escapes	Ratio (%)
Bilateral ablation			
Fish 1	10	7	70.0
Fish 2	3	1	33.3
Fish 3	9	1	11.1
Fish 4	23	4	17.4
Fish 5	9	0	0.0
Fish 6	21	11	52.4
Fish 7	25	4	16.0
			28.6 average
Unilateral ablation			
Fish 8	5^a	2	40.0
Fish 9	6^a	5	83.3
Fish 10	5^a	1	20.0
Fish 11	2^a	1	50.0
Fish 12	3^a	1	33.3
Fish 13	8^a	2	25.0
Fish 14	5^a	0	0.0
			36.0 average

Table 1. Frequency of impaired escapes in CoLo-ablated larvae.

In fish 6 and fish 7, CoLos located caudal to the 11th segment were ablated. For all the other fish, ablations were carried out against CoLos located caudal to the 7th segment. [a]In the unilateral ablation experiments (fish 8-14), impaired escapes occurred only toward the side of the ablation. Therefore, in the "Number of total escapes", only those escapes that occurred in that direction were counted.

CONCLUDING REMARKS

Neural circuits are composed of many types of neurons. To understand neural circuitry, each class of neuron has to be examined individually. I took several approaches to accomplish this. For my V0 studies, the Cre/loxP system was combined with neurotransmitter-specific promoters. A transient expression system was also utilized. These labeling methods worked successfully to reveal the fine morphology of each class of V0 neuron. For V0-iB neurons, I performed a physiological analysis, and obtained data that strongly suggest that V0-iB neurons play an important role in the left-right alteration of body movements during swimming. It should be possible to examine other classes of V0 neurons using the same methodology. Such studies will provide a wealth of information about the organization of spinal locomotor circuits, including the role of crossed excitation during locomotion.

In the CoLo study, enhancer-trap lines of zebrafish were screened. The Tol-056 line, identified during screening, provided an ideal situation: only one class of neuron was labeled by GFP. This line allowed me to perform detailed morphological, electrophysiological, and functional analyses of CoLo neurons. The results showed that CoLos, which occur only once per hemisegment, play a very important role in escape behavior. CoLos can, in a broad sense, be categorized into commissural neurons that provide inhibition to the contralarateral side, like V0-iBs. However, the functions of CoLos and V0-iBs are quite different when considered in a behavioral context: CoLos are only involved in escape movements. Thus, the CoLo study provides an example of a distinct class of neuron that is used in a distinct form of locomotion within spinal locomotor circuitry. I think this is one of the clearest examples of such cases, and in this

sense, the CoLo study is of general importance to the neuroscience field.

Throughout this study, the transparency of the larval body has been critical for performing most of the experiments, including morphological analysis, targeting patch recordings, and laser ablations. The transparency of the body is also perfectly suited for applying recently developed optogenetic tools, by which researchers can activate or inactivate neuronal activity with light (Douglass et al., 2008; Arrenberg et al., 2009). These new tools, combined with the existing techniques employed in this study, should be very powerful for investigating locomotor circuits in zebrafish. I expect that future studies in zebrafish will reveal many more details of organization and computation in locomotor circuitry, which in turn will provide useful information for the study of locomotor circuits in all vertebrates.

REFERENCES

Al-Mosawie A, Wilson JM, Brownstone RM (2007) Heterogeneity of V2-derived interneurons in the adult mouse spinal cord. Eur J Neurosci 26:3003-3015.

Ali DW, Buss RR, Drapeau P (2000) Properties of miniature glutamatergic EPSCs in neurons of the locomotor regions of the developing zebrafish. J Neurophysiol 83:181-191.

Arrenberg AB, Del Bene F, Baier H (2009) Optical control of zebrafish behavior with halorhodopsin. Proc Natl Acad Sci U S A 106:17968-17973.

Baba SA, Mogami Y (1985) An approach to digital image analysis of bending shapes of eukaryotic flagella and cilia. Cell Motility 5:475-489.

Bernardos RL, Raymond PA (2006) GFAP transgenic zebrafish. Gene Expr Patterns 6:1007-1013.

Bernhardt RR, Chitnis AB, Lindamer L, Kuwada JY (1990) Identification of spinal neurons in the embryonic and larval zebrafish. J Comp Neurol 302:603-616.

Bhatt DH, Otto SJ, Depoister B, Fetcho JR (2004) Cyclic AMP-induced repair of zebrafish spinal circuits. Science 305:254-258.

Briscoe J, Pierani A, Jessell TM, Ericson J (2000) A homeodomain protein code specifies progenitor cell identity and neuronal fate in the ventral neural tube. Cell 101:435-445.

Brown TG (1914) On the nature of the fundamental activity of the nervous centres; together with an analysis of the conditioning of rhythmic activity in progression, and a theory of the evolution of function in the nervous system. J Physiol 48:18-46.

Buchanan JT (1982) Identification of interneurons with contralateral, caudal axons in the lamprey spinal cord: synaptic interactions and morphology. J Neurophysiol 47:961-975.

Buchanan JT, Cohen AH (1982) Activities of identified interneurons, motoneurons, and muscle fibers during fictive swimming in the lamprey and effects of reticulospinal and dorsal cell stimulation. J Neurophysiol 47:948-960.

Burgess HA, Granato M (2007) Sensorimotor gating in larval zebrafish. J Neurosci 27:4984-4994.

Buss RR, Drapeau P (2001) Synaptic drive to motoneurons during fictive swimming in the developing zebrafish. J Neurophysiol 86:197-210.

Casagrand JL, Guzik AL, Eaton RC (1999) Mauthner and reticulospinal responses to the onset of acoustic pressure and acceleration stimuli. J Neurophysiol 82:1422-1437.

Cina C, Hochman S (2000) Diffuse distribution of sulforhodamine-labeled neurons during serotonin-evoked locomotion in the neonatal rat thoracolumbar spinal cord. J Comp Neurol 423:590-602.

Crone SA, Zhong G, Harris-Warrick R, Sharma K (2009) In mice lacking V2a interneurons, gait depends on speed of locomotion. J Neurosci 29:7098-7109.

Crone SA, Quinlan KA, Zagoraiou L, Droho S, Restrepo CE, Lundfald L, Endo T, Setlak J, Jessell TM, Kiehn O, Sharma K (2008) Genetic ablation of V2a ipsilateral interneurons disrupts left-right locomotor coordination in mammalian spinal cord. Neuron 60:70-83.

Dai X, Noga BR, Douglas JR, Jordan LM (2005) Localization of spinal neurons activated during locomotion using the c-fos immunohistochemical method. J Neurophysiol 93:3442-3452.

Diamond J (1971) The Mauthner cell. In: Fish Physiology. Vol. V, 0 Edition (Hoar WS, Randall DJ, eds), pp 265-346. New York: Academic Press.

Doe CQ, Technau GM (1993) Identification and cell lineage of individual neural precursors in the Drosophila CNS. Trends Neurosci 16:510-514.

Douglass AD, Kraves S, Deisseroth K, Schier AF, Engert F (2008) Escape behavior elicited by single, channelrhodopsin-2-evoked spikes in zebrafish somatosensory neurons. Curr Biol 18:1133-1137.

Drapeau P, Ali DW, Buss RR, Saint-Amant L (1999) In vivo recording from identifiable neurons of the locomotor network in the developing zebrafish. J Neurosci Methods 88:1-13.

Eaton RC (1984) In: Neural mechanisms of startle behavior, 0 Edition, p 0. New York: Plenum Press.

Eaton RC, Lavender WA, Wieland CM (1981) Identification of Mauthner-initiated response patterns in goldfish: Evidence from simultaneous cinematography and electrophysiology. JCompPhysiol 144:521-531.

Eaton RC, DiDomenico R, Nissanov J (1988) Flexible body dynamics of the goldfish C-start: Implications for reticulospinal command mechanisms. JNeurosci 8:2758-2768.

Eaton RC, Lee RK, Foreman MB (2001) The Mauthner cell and other identified neurons of the brainstem escape network of fish. Prog Neurobiol 63:467-485.

Fetcho JR (1990) Morphological variability, segmental relationships, and functional role of a class of commissural interneurons in the spinal cord of goldfish. J Comp Neurol 299:283-298.

Fetcho JR (1991) Spinal network of the Mauthner cell. Brain Behav Evol 37:298-316.

Fetcho JR (2007) The utility of zebrafish for studies of the comparative biology of motor systems. J Exp Zool B Mol Dev Evol 308:550-562.

Fetcho JR, Faber DS (1988) Identification of motoneurons and interneurons in the spinal network for escapes initiated by the mauthner cell in goldfish. J Neurosci 8:4192-4213.

Fetcho JR, Higashijima S, McLean DL (2008) Zebrafish and motor control over the last decade. Brain Res Rev 57:86-93.

Fogarty M, Richardson WD, Kessaris N (2005) A subset of oligodendrocytes generated from radial glia in the dorsal spinal cord. Development 132:1951-1959.

Goulding M (2009) Circuits controlling vertebrate locomotion: moving in a new direction. Nat Rev Neurosci 10:507-518.

Goulding M, Lamar E (2000) Neuronal patterning: Making stripes in the spinal cord. Curr Biol 10:R565-568.

Gribble SL, Nikolaus OB, Dorsky RI (2007) Regulation and function of Dbx genes in the zebrafish spinal cord. Dev Dyn 236:3472-3483.

Grillner S, Zangger P (1979) On the central generation of locomotion in the low spinal cat. Exp Brain Res 34:241-261.

Grillner S, Parker D, el Manira A (1998) Vertebrate locomotion--a lamprey perspective. Ann N Y Acad Sci 860:1-18.

Hale ME, Ritter DA, Fetcho JR (2001) A confocal study of spinal interneurons in living larval zebrafish. J Comp Neurol 437:1-16.

Halloran MC, Sato-Maeda M, Warren JT, Su F, Lele Z, Krone PH, Kuwada JY, Shoji W (2000) Laser-induced gene expression in specific cells of transgenic zebrafish. Development 127:1953-1960.

Hatta K, Korn H (1999) Tonic inhibition alternates in paired neurons that set direction of fish escape reaction. Proc Natl Acad Sci U S A 96:12090-12095.

Higashijima S (2008) Transgenic zebrafish expressing fluorescent proteins in central nervous system neurons. Dev Growth Differ 50:407-413.

Higashijima S, Mandel G, Fetcho JR (2004a) Distribution of prospective glutamatergic, glycinergic, and GABAergic neurons in embryonic and larval zebrafish. J Comp Neurol 480:1-18.

Higashijima S, Schaefer M, Fetcho JR (2004b) Neurotransmitter properties of spinal interneurons in embryonic and larval zebrafish. J Comp Neurol 480:19-37.

Higashijima S, Masino MA, Mandel G, Fetcho JR (2004c) Engrailed-1 expression marks a primitive class of inhibitory spinal interneuron. J Neurosci 24:5827-5839.

Jayne BC, Lauder GV (1993) Red and white muscle activity and kinematics of the escape response of the bluegill sunfish during swimming. JCompPhysiolA 173:495-508.

Jessell TM (2000) Neuronal specification in the spinal cord: inductive signals and transcriptional codes. Nat Rev Genet 1:20-29.

Kawakami K (2004) Transgenesis and gene trap methods in zebrafish by using the Tol2 transposable element. Methods Cell Biol 77:201-222.

Kiehn O (2006) Locomotor circuits in the mammalian spinal cord. Annu Rev Neurosci 29:279-306.

Kiehn O, Butt SJ (2003) Physiological, anatomical and genetic identification of CPG neurons in the developing mammalian spinal cord. Prog Neurobiol 70:347-361.

Kimura Y, Okamura Y, Higashijima S (2006) alx, a zebrafish homolog of Chx10, marks ipsilateral descending excitatory interneurons that participate in the regulation of spinal locomotor circuits. J Neurosci 26:5684-5697.

Kimura Y, Satou C, Higashijima S (2008) V2a and V2b neurons are generated by the final divisions of pair-producing progenitors in the zebrafish spinal cord. Development 135:3001-3005.

Kjaerulff O, Kiehn O (1996) Distribution of networks generating and coordinating locomotor activity in the neonatal rat spinal cord in vitro: a lesion study. J Neurosci 16:5777-5794.

Kohashi T, Oda Y (2008) Initiation of Mauthner- or non-Mauthner-mediated fast escape evoked by different modes of sensory input. J Neurosci 28:10641-10653.

Korn H, Faber DS (2005) The Mauthner cell half a century later: a neurobiological model for decision-making? Neuron 47:13-28.

Kwan AC, Dietz SB, Webb WW, Harris-Warrick RM (2009) Activity of Hb9 interneurons during fictive locomotion in mouse spinal cord. J Neurosci 29:11601-11613.

Lanuza GM, Gosgnach S, Pierani A, Jessell TM, Goulding M (2004) Genetic identification of spinal interneurons that coordinate left-right locomotor activity necessary for walking movements. Neuron 42:375-386.

Lee EC, Yu D, Martinez de Velasco J, Tessarollo L, Swing DA, Court DL, Jenkins NA, Copeland NG (2001) A highly efficient Escherichia coli-based chromosome engineering system adapted for recombinogenic targeting and subcloning of BAC DNA. Genomics 73:56-65.

Liao JC, Fetcho JR (2008) Shared versus specialized glycinergic spinal interneurons in axial motor circuits of larval zebrafish. J Neurosci 28:12982-12992.

Matsuzaki F (2000) Asymmetric division of Drosophila neural stem cells: a basis for neural diversity. Curr Opin Neurobiol 10:38-44.

McLean DL, Fan J, Higashijima S, Hale ME, Fetcho JR (2007) A topographic map of recruitment in spinal cord. Nature 446:71-75.

McLean DL, Masino MA, Koh IY, Lindquist WB, Fetcho JR (2008) Continuous shifts in the active set of spinal interneurons during changes in locomotor speed. Nat Neurosci 11:1419-1429.

Mizuguchi R, Kriks S, Cordes R, Gossler A, Ma Q, Goulding M (2006) Ascl1 and Gsh1/2 control inhibitory and excitatory cell fate in spinal sensory interneurons. Nat Neurosci 9:770-778.

Moran-Rivard L, Kagawa T, Saueressig H, Gross MK, Burrill J, Goulding M (2001) Evx1 is a postmitotic determinant of v0 interneuron identity in the spinal cord. Neuron 29:385-399.

Nabekura J, Katsurabayashi S, Kakazu Y, Shibata S, Matsubara A, Jinno S, Mizoguchi Y, Sasaki A, Ishibashi H (2004) Developmental switch from GABA to glycine release in single central synaptic terminals. Nat Neurosci 7:17-23.

Nagayoshi S, Hayashi E, Abe G, Osato N, Asakawa K, Urasaki A, Horikawa K, Ikeo K, Takeda H, Kawakami K (2008) Insertional mutagenesis by the Tol2 transposon-mediated enhancer trap approach generated mutations in two developmental genes: tcf7 and synembryn-like. Development 135:159-169.

Nissanov J, Eaton RC, DiDomenico R (1990) The motor output of the Mauthner cell, a reticulospinal command neuron. Brain Res 517:88-98.

O'Brien J, Bruzzone R, White TW, Al-Ubaidi MR, Ripps H (1998) Cloning and expression of two related connexins from the perch retina define a distinct subgroup of the connexin family. J Neurosci 18:7625-7637.

O'Malley DM, Kao Y-H, Fetcho JR (1996) Imaging the functional organization of zebrafish hindbrain segments during escape behaviors. Neuron 17:1145-1155.

Peng CY, Yajima H, Burns CE, Zon LI, Sisodia SS, Pfaff SL, Sharma K (2007) Notch and MAML signaling drives Scl-dependent interneuron diversity in the spinal cord. Neuron 53:813-827.

Pereda A, O'Brien J, Nagy JI, Bukauskas F, Davidson KG, Kamasawa N, Yasumura T, Rash JE (2003) Connexin35 mediates electrical transmission at mixed synapses on Mauthner cells. J Neurosci 23:7489-7503.

Pierani A, Moran-Rivard L, Sunshine MJ, Littman DR, Goulding M, Jessell TM (2001) Control of interneuron fate in the developing spinal cord by the progenitor homeodomain protein Dbx1. Neuron 29:367-384.

Rash JE, Yasumura T, Dudek FE, Nagy JI (2001) Cell-specific expression of connexins and evidence of restricted gap junctional coupling between glial cells and between neurons. J Neurosci 21:1983-2000.

Ritter DA, Bhatt DH, Fetcho JR (2001) In vivo imaging of zebrafish reveals differences in the spinal networks for escape and swimming movements. J Neurosci 21:8956-8965.

Roberts A (2000) Early functional organization of spinal neurons in developing lower vertebrates. Brain Res Bull 53:585-593.

Roberts A, Clarke JDW (1982) The neuroanatomy of an amphibian embryo spinal cord. PhilTransRSocB 296:195-212.

Roberts A, Li WC, Soffe SR (2008) Roles for inhibition: studies on networks controlling swimming in young frog tadpoles. J Comp Physiol A Neuroethol Sens Neural Behav Physiol 194:185-193.

Sapir T, Geiman EJ, Wang Z, Velasquez T, Mitsui S, Yoshihara Y, Frank E, Alvarez FJ, Goulding M (2004) Pax6 and engrailed 1 regulate two distinct aspects of renshaw cell development. J Neurosci 24:1255-1264.

Saueressig H, Burrill J, Goulding M (1999) Engrailed-1 and netrin-1 regulate axon pathfinding by association interneurons that project to motor neurons. Development 126:4201-4212.

Seo HC, Nilsen F, Fjose A (1999) Three structurally and functionally conserved Hlx genes in zebrafish. Biochim Biophys Acta 1489:323-335.

Shiba K, Ohmuro J, Mogami Y, Nishigaki T, Wood CD, Darszon A, Tatsu Y, Yumoto N, Baba SA (2005) Sperm-activating peptide induces asymmetric flagellar bending in sea urchin sperm. Zoolog Sci 22:293-299.

Shirasaki R, Pfaff SL (2002) Transcriptional codes and the control of neuronal identity. Annu Rev Neurosci 25:251-281.

Svoboda KR, Fetcho JR (1996) Interactions between the neural networks for escape and swimming in goldfish. J Neurosci 16:843-852.

Takahashi M, Narushima M, Oda Y (2002) In vivo imaging of functional inhibitory networks on the mauthner cell of larval zebrafish. J Neurosci 22:3929-3938.

Urasaki A, Morvan G, Kawakami K (2006) Functional dissection of the Tol2 transposable element identified the minimal cis-sequence and a highly repetitive sequence in the subterminal region essential for transposition. Genetics 174:639-649.

Wood CD, Nishigaki T, Furuta T, Baba SA, Darszon A (2005) Real-time analysis of the role of Ca(2+) in flagellar movement and motility in single sea urchin sperm. J Cell Biol 169:725-731.

Yasargil GM, Diamond J (1968) Startle-response in teleost fish: an elementary circuit for neural discrimination. Nature 220:241-243.

Yasargil GM, Sandri C (1987) Morphology of the Mauthner axon inhibitory system in tench (Tinca tinca L.) spinal cord. NeurosciLett 81:63-68.

Yasargil GM, Sandri C (1990) Topography and ultrastructure of commissural interneurons that may establish reciprocal inhibitory connections of the Mauthner axons in the spinal cord of the tench, Tinca tinca L. JNeurocytol 19:111-126.

Zar JH (2009) Biostatistical Analysis. Person Education International 5th edition.

Zottoli SJ (1977) Correlation of the startle reflex and Mauthner cell auditory responses in unrestrained goldfish. JExpBiol 66:243-254.

ACKNOWLEDGEMENT

Though only my name appears on the cover of this dissertation, a great many people have contributed to its production. I owe my gratitude to all those people who have made this dissertation possible.

First and foremost, I would like to gratefully and sincerely thank my supervisor, Dr. Shin-ichi Higashijima for his guidance, understanding, kindness and patience throughout my graduate studies during five years. I have been amazingly fortunate to have an advisor who gave me the freedom to explore on my own and at the same time the guidance to recover when my steps faltered. His mentorship was paramount in providing a well rounded experience consistent with my long-term career goals.

I am grateful to Drs. Yoichi Oda and Tsunehiko Kohashi for their support of behavior experiments. It was difficult to complete this project without their practical advice and experimental help. I would also like to thank all the members of the Oda research group for their kindness.

I would like to thank Drs. Hiroyuki Takeda and Kazuki Horikawa for providing me a great opportunity to perform screening from their enhancer trap lines. Without them, CoLo project could not have been started.

I am grateful to Dr. David McLean for his practical advice. I am also thankful to him for reading my thesis, commenting on my views and helping me understand and enrich my ideas.

I would like to thank the members of the Higashijima research group, especially, Dr. Yukiko Kimura, with whom I worked closely and puzzled over many of

the same problems, for the many valuable discussions. I am also grateful to all the member of the Okamura and Yoshimura research groups for numerous discussions, some much needed humor, and friendly environment.

My partner, Yoshihito Takeuchi, and many friends have helped me stay sane through these difficult years. Their support and care helped me overcome setbacks and stay focused on my graduate study.

Finally, I would like to thank my parents for encouraging and supporting me throughout my studies.